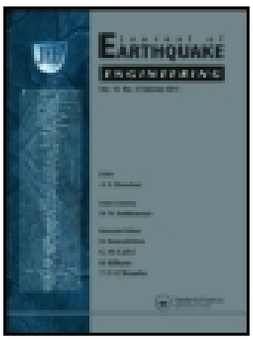

Journal of Earthquake Engineering

ISSN: 1363-2469 (Print) 1559-808X (Online) Journal homepage: http://www.tandfonline.com/loi/ueqe20

Seismic Assessment of Existing Hollow Circular Reinforced Concrete Bridge Piers

Paolino Cassese, Maria Teresa De Risi & Gerardo Mario Verderame

To cite this article: Paolino Cassese, Maria Teresa De Risi & Gerardo Mario Verderame (2018): Seismic Assessment of Existing Hollow Circular Reinforced Concrete Bridge Piers, Journal of Earthquake Engineering, DOI: 10.1080/13632469.2018.1471430

To link to this article: https://doi.org/10.1080/13632469.2018.1471430

Accepted author version posted online: 30 Apr 2018.

SEISMIC ASSESSMENT OF EXISTING HOLLOW CIRCULAR REINFORCED CONCRETE BRIDGE PIERS

Paolino Cassese [(*)], Maria Teresa De Risi, Gerardo Mario Verderame

paolino.cassese@unina.it, mariateresa.derisi@unina.it, verderam@unina.it

University of Naples Federico II
Department of Structures for Engineering and Architecture
Via Claudio, 21, Naples, Italy

(*) corresponding author

ABSTRACT

Experimental works in literature have paid proper attention to the seismic response of hollow circular piers only quite recently, despite their widespread use in existing bridges. More attention should be certainly paid to these elements to reliably assess their seismic capacity.

Herein, experimental cyclic tests on two scaled reinforced concrete piers with hollow circular cross section, representative of typical existing Italian bridges, are carried out. Depending on the aspect ratio, flexure and flexure-shear failure modes have been observed. Design criteria, adopted setup, experimental response and damage evolution are presented and discussed.

A focus on shear-critical piers has been performed, collecting a proper experimental database of tests from literature. The very few specific shear strength models existing in literature and main models by codes are compared with the collected data. Model by Ranzo and Priestley (2001), also in conjunction with proposal by Turmo et al. (2009), has finally shown promising results.

Keywords: *existing reinforced concrete bridge piers; hollow circular cross section; cyclic tests; deformability contributions; seismic assessment; shear capacity.*

1 INTRODUCTION

Seismic assessment of existing bridge structures is a key issue especially in regions where most of bridges have been realized without proper rules for earthquake resistant structures, generally designed for gravity loads only or according to obsolete seismic codes. Furthermore, hollow section piers are a very popular structural solution for reinforced concrete (RC) bridge structures due to their economical convenience and higher efficiency with respect to solid sections. Nowadays, the most updated seismic codes require to concentrate energy dissipation in ductile flexural hinges at the base of the bridge piers [Priestley et al., 1996], and avoid brittle shear failure of piers. Vice-versa, existing hollow piers are generally characterized by poor structural details, limited confined concrete core, crucial to seismic energy dissipation, and a deeper degradation of shear resisting mechanisms [Kim et al., 2012]. Their premature collapse is often due to a very limited shear capacity [De Risi et al., 2017]. Moreover, seismic response of hollow RC piers generally exhibits high shear deformability contribution to the global top displacement [Delgado et al., 2009].

The starting point for this study is a comprehensive literature review about the investigated structural typology, as reported in section 1.1.

1.1 Literature review

1.1.1 Experimental works from literature

Despite their widespread use, experimental works in literature have paid proper attention to the seismic response of hollow circular piers only quite recently. In fact, some experimental campaigns on RC members with hollow-core circular cross section and *double* reinforcement layer (inner and outer) have been found in literature since late ‘80s. A first experimental study, on six specimens, by [Whittaker et al., 1987] was focused on seismic response of scaled RC hollow circular members characterized by two layers of longitudinal reinforcement and well-detailed transverse reinforcement, proving that this kind of members were able to exhibit a ductile behaviour similarly to well-detailed solid members. Five cyclic tests on bridge piers with large diameter were later performed by [Yeh et al., 2001] and [Cheng et al., 2003], focusing on the effect of the transverse reinforcement amount and layout on the cyclic performance. Results showed that the lack of the internal transverse

reinforcement between the two steel layers might produce failure in tension of some longitudinal steel bars at the bottom of the column after concrete crushing, buckling during compression cycles, and flexure-shear failure if external transverse reinforcement is not sufficient.

Other researchers focused on hollow circular sections with a *single* longitudinal (and transverse) reinforcement layer, widely used more recently since time and cost needed to place double reinforcement was not counterbalanced by significantly improved performance [Hoshikuma and Priestley, 2000]. The principal goal of these experimental studies was the analysis of the effect on flexural behaviour of the absence of the inner reinforcing layer. First studies [Zahn et al., 1990] showed that the failure was announced by early vertical splitting and crushing of the concrete on the inside face. Despite the lack of confinement on the inner face, in case of low amounts of longitudinal reinforcement, low levels of axial load and reasonably thick wall, a sufficient ductile behaviour was observed, also for this structural solution. These results were then extended and confirmed by [Hoshikuma and Priestley, 2000] - for hollow circular columns with thin walls and realistic axial load levels and reinforcement ratios - and by [Lee et al., 2015].

Furthermore, hollow circular piers could be very vulnerable to shear failure when subjected to cyclic loads, because of the absence of a proper resistant concrete core. This issue is certainly of particular importance for existing structures, generally characterized by low strength concrete and transverse reinforcement amount. Moreover, the shear strength degradation due to the ductility demand deepens this problem. First, [Regis, 1990] performed four monotonic tests on simple supported beams subjected to two symmetric shear forces, with and without axial compression, characterized by ordinary strength concrete and poor reinforcement details. Authors experimentally observed failure in shear before flexural yielding for all the tests. [Kishida et al., 1998] carried-out an experimental study on a particular typology of hollow circular members, not representative of existing bridge piers. In particular, 58 pre-tensioned spun high-strength concrete piles (PHC pile) with hollow circular cross section were tested under monotonically increasing lateral load, different for thickness, longitudinal and transverse steel ratio, and steel yielding strength. Some of them were filled with concrete into the hollow part. As a result, the increasing of the amount of transverse (spiral) reinforcement improved the shear strength, as expected; the filling with concrete increased the

ultimate strength, but brittle failures were not avoided. Later, [Ranzo and Priestley, 2001] conducted cyclic tests on three large size bridge piers with one external layer of longitudinal and spiral reinforcement, different for axial load and longitudinal reinforcement levels. Two of them failed in shear after flexural yielding. [Turmo et al, 2009] performed four experimental tests on hollow circular beams, simply supported, under monotonic transverse load applied at mid-span. The specimens were identical, except for slight differences in concrete compressive strength, and presented very similar responses characterised by the occurrence of a shear failure. More recently, [Völgyi et al., 2014a] carried-out an experimental programme of 45 tests on hollow circular RC members with thick-walled and high-strength concrete, under monotonic loading only.

In summary, very few experimental tests representative of existing RC piers exists in literature, especially on shear-critical piers. Moreover, the latter are generally characterised by very high value of concrete compressive strength. Based on some of these experimental works, shear strength models have been proposed, as reported and discussed in section 1.1.2.

1.1.2 Shear strength models from literature and codes

The detection of the shear failure is a key issue for low-standard existing RC piers, in particular for hollow-core members, for which, no seismic code provides ad-hoc formulations, actually failing to recognise the distinctive features of this structural typology with respect to ordinary solid members. Main existing degrading shear strength models by codes have been calibrated on experimental results of members with solid cross section, rectangular and circular in particular [Aschheim and Moehle, 1992; Kowalsky and Priestley, 2000; Sezen and Moehle, 2004; Biskinis et al., 2004]. Nevertheless, shear-resisting mechanisms of hollow RC members may be significantly different, as highlighted by several experimental studies [Ranzo and Priestley, 2001; Calvi et al., 2005; Kim et al., 2012; Cassese et al. 2017]. In particular, the reduced effective concrete area resisting to the shear force, the limited thickness generally characterizing the hollow piers very sensitive to concrete degradation mechanisms, and the effectiveness of the inclined strut due to combined axial, among others, can still be considered as open issues, dramatically influencing the assessment of the shear strength of RC hollow members subjected to cyclic loads (as seismic ones).

Despite these remarks, no ad-hoc degrading shear strength model is present in literature, calibrated for the assessment of hollow circular RC members with ordinary concrete strength (typical of existing bridge piers). Some specialized shear-strength models have been calibrated on experimental results of high-strength concrete hollow circular members and does not account for any degradation effect due to increasing ductility demand [Jensen and Hoang, 2010; Völgyi et al., 2014b].

In particular, the shear strength model derived by [Völgyi et al., 2014b] – able to consider several potential failure sections with different location and shape – does not consider shear strength degradation and it is unfortunately not so straightforward to apply, since the concrete contribution has to be prior evaluated by means of a finite elements analysis.

The proposal of a proper procedure for the evaluation of the shear strength for hollow circular members was also carried-out by [Jensen and Hoang, 2010], without considering shear strength degradation, based on the experimental results on high-strength concrete piles tested by [Kishida et al., 1998]. [Ranzo and Priestley, 2001], starting from model proposed by [Kowalsky and Priestley, 2000] for solid circular section piers, first proposed a modification of the concrete contribution, only, to shear strength, on the basis of two experimental tests carried out on hollow circular RC bridge piers with helical transverse reinforcement. Later, [Turmo et al, 2009] proposed a theoretical study aiming to define the transverse reinforcement contribution, only, specifically for hollow circular members.

The latter three studies on shear strength from literature – the only ones dedicated to hollow-core circular members from literature and implementable without a-priori finite element analyses – are briefly described in the following, together with some formulations provided by the main technical codes adopted in Italy [C617, 2009], Europe [CEN, 2005], and USA [FHWA, 2006], representative of what practitioners should do to assess seismic performance of existing RC bridge piers.

Ranzo and Priestley, 2001 (hereinafter referred to as "RP")

The model by [Ranzo and Priestley, 2001] represents the specification to hollow circular members of the model proposed by [Kowalsky and Priestley, 2000] for solid circular section piers. In particular, the original UCSD model [Priestley et al., 1994] has been validated on the basis on a dataset of 47

columns with solid circular cross section failing in shear or flexure-shear. The RP revision has been proposed based on the experimental results of only two columns, as highlighted previously.

The shear strength V_{RP} is expressed as the sum of three contributions, corresponding to: *(i)* the axial load (N) component due to the formation of an inclined strut in the column, V_N; *(ii)* the concrete mechanism component, V_c; and *(iii)* the truss mechanism component due to transverse reinforcement contribution, V_w. In particular, differently from the Original UCSD model [Priestley et al., 1994] from which it was born, V_c accounts for the influence of column aspect ratio and longitudinal steel ratio on concrete mechanisms contributions. More in details, the modifications with respect to the original UCSD model concerns the computation of *(i)* the effective shear area (A_e) and *(ii)* of the neutral axis depth (x), by means of the coefficients (γ) and (β), respectively. In Eqs. (1-4), all the above-mentioned shear contributions are specified.

$$\begin{aligned} V_{RP} &= V_N + (k \cdot V_c) + V_w \\ V_N &= \frac{(D_e - x)}{2L_V} N \\ V_c &= \alpha \cdot \beta \cdot \sqrt{f_c}(0.8A_e) \\ V_w &= \frac{\pi}{4} \cdot \frac{n_\Phi A_\Phi}{s} f_{yw} \cdot (D_e - x - c) \cdot \cot(30°) \end{aligned} \quad (1)$$

$$A_e = \frac{(1+\gamma^2)(1-\gamma)}{(1-\gamma^3)} A_c \text{; with } \gamma = \frac{D_e - 2t_w}{D_e} \quad (2)$$

$$\alpha = \min\left(1.5; \max\left(1.0; 3 - \frac{L_V}{D_e}\right)\right) \quad (3)$$

$$\begin{aligned} \beta &= \min(1.0; 0.5 + 20\rho_l) \text{ if } x \geq t_w \\ \beta &= 0.5 + 20\frac{A_l}{\pi D_e^{\,2}/4} \quad \text{if } x < t_w \end{aligned} \quad (4)$$

where (x) is the depth of the compressed zone (evaluated at nominal flexural capacity); (f_c) and (f_{yw}) are concrete compressive strength and steel yielding strength, respectively; (c), (L_v), (D_e) and (t_w) represent concrete cover, shear length, external diameter and web thickness, respectively; (A_l) is the longitudinal reinforcement area and (ρ_l) represents the geometrical longitudinal reinforcement ratio (evaluated with respect to the circular crown); (A_Φ) is the area of a single steel hoop or spiral; (s) is the spacing of the stirrups or the pitch of the spiral; (n_Φ) is the number of effective legs in the cross

section; and (μ) is the ductility demand. The shear strength degradation due to ductility demand (μ) is taken into account through the coefficient (k), which multiplies the concrete contribution and varies linearly between 0.29 (non-degraded shear strength) and 0.05 for (μ) between 2.0 and 8.0 (for the uniaxial case).

Turmo et al., 2009 (hereinafter referred to as "T")

[Turmo et al., 2009] presented a thorough theoretical study about the evaluation of the transverse reinforcement contribution (V_w) only to the shear strength of RC members characterized by circular cross section, both with solid or hollow-core, with spiral or discontinuous reinforcement. The Authors proposed a modified version of the classical Ritter-Mörsh truss model, providing two factors (λ) and (χ) to take into account the efficiency of the transverse reinforcement in the longitudinal and transverse direction, respectively, as reported in Eqs. (5-6):

$$V_w = \lambda \cdot \chi \cdot \frac{n_\Phi A_\Phi}{p} f_{yw} \cdot z \cdot \cot(\theta) \quad \text{(for helical transverse reinforcement)}$$
$$V_w = \lambda \cdot \chi \cdot \frac{n_\Phi A_\Phi}{s} f_{yw} \cdot z \cdot \cot(\theta) \quad \text{(for circular transverse reinforcement)} \tag{5}$$

$$\lambda = \frac{1}{\sqrt{\left(\frac{p}{2\pi R'}\right)^2 + 1}} \tag{6}$$

where (θ) is the angle between the critical diagonal crack and the longitudinal axis; (p) is the pitch of the continuous spiral, (R′) is the radius of the circular or helical transverse reinforcement; (z) is the internal lever arm. The efficiency factor in transversal direction (χ) is assumed equal to 1.0 for hollow circular members, reinforced with both circular or spiral ties. The efficiency coefficient in longitudinal direction (λ) is assumed equal to the unity when circular ties are adopted; whereas, in the case of continuous spiral, the factor (λ) is evaluated according to Eq. (6) as a function of the pitch-to-stirrups circumference ratio.

Jensen and Hoang, 2010 (hereinafter referred to as "JH")

[Jensen and Hoang, 2010] proposed a plasticity-based procedure for the assessment of the shear strength (V_{JH}) of RC piers and piles with hollow circular cross section, under combined shear and

axial compression. In particular, this model has been validated on the experimental results of 60 tests for failing in shear. Nevertheless, 56 test specimens [Kishida et al., 1998] were characterized by very high-strength concrete. The proposed procedure is briefly summarized below.

Depending on the level of the axial load, two distinct failure modes in shear are considered: "sliding failure in cracked concrete" (for low axial load level) and "failure in uncracked concrete" (for high axial load level). Therefore, first, check is necessary to establish if the member is cracked, by assuming a simple plasticity-based cracking criterion [Zhang, 1997]. Such criterion identifies the cracking load (V_{cr}) for solid circular beams, which can be also applied to hollow members [Jensen and Hoang, 2009], as in Eq. (7):

$$V_{cr} = \frac{\frac{1}{2} f_{tef} A_c \left[1 + \left(\frac{m}{D_e} \right)^2 \right] + \frac{1}{2} N}{L_v / D_e}; \quad f_{tef} = 0.156 f_c^{2/3} \left(\frac{D_e}{0.1} \right)^{-0.3} \tag{7}$$

where (f_{tef}) is the effective tensile strength, (A_c) is the concrete cross section area, (m) is the longitudinal projection of the critical diagonal crack (forming an angle θ with the longitudinal axis), and all the other terms have been defined above. The shear strength for a member sensitive to a crack sliding failure is determined by the plasticity-based crack-sliding model, as reported in Eq. (8):

$$V_{JH,cr} = \frac{1}{2} \nu_s \nu_0 f_c \left(\sqrt{1 + \left(\frac{m}{D_e} \right)^2} - \frac{m}{D_e} \right) A_c + \frac{\pi}{4} \frac{n_\Phi A_\Phi f_{yw}}{s} (D_e - 2c) \left(\frac{m}{D_e} \right) C \tag{8}$$

where (ν_o) is the concrete effectiveness factor (plastic theory), (ν_s) is an additional effectiveness factor accounting for the reduction of the cohesion due to sliding crack, and (C) is a factor taking into account the discrete spacing of the hoops.

In the case of large compressive normal force (N), the shear failure is assumed to take place in a sudden diagonal crack, formed in uncracked concrete. In this case, the shear strength ($V_{JH,un}$) can be computed as in Eq. (8) by assuming (ν_s) equal to the unity (no crack sliding failure).

The expressions of (V_{cr}), ($V_{JH,cr}$) and ($V_{JH,un}$) define three curves depending on the angle of the critical diagonal crack (θ), or equivalently, its projection on the longitudinal axis (m). The final value of the shear strength can be finally defined as the minimum value between shear value corresponding to the

intersection of ($V_{JH,cr}$) and (V_{cr}) and the upper bound of ($V_{JH,un}$), within the range of interest [$3/4D_e \leq m \leq L_v$].

CEN 2005 (hereinafter referred to as "EC8")

The European code [CEN, 2005] provides a formulation for the evaluation of the shear strength of RC columns (V_{EC8}) derived from [Biskinis et al., 2004]. This model is assumed as the reference shear capacity model for design and assessment of bridges by some Authors [Fardis and Pinto, 2007; Pinto et al., 2005]. This empirical-based formulation provides the shear strength capacity of RC members failing in shear by diagonal tension prior to or following flexural yielding. Hollow rectangular and solid circular columns were included in the database, partly representative of existing bridge piers without seismic details, but no hollow circular members are present within this database. Also in this case, the shear strength is expressed as the sum of the three contributions respectively corresponding to axial load, concrete and transverse steel truss contribution, according to Eq. (9):

$$
\begin{aligned}
&V_{EC8} = V_N + k \cdot (V_c + V_w) \\
&V_N = \frac{(D_e - x)}{2L_V} \min(N; 0.55 A_c f_c) \\
&V_c = 0.16 \max(0.5; 100\rho_l) \left(1 - 0.16 \min\left(5; \frac{L_V}{D_e}\right)\right) \sqrt{f_c} A_c \\
&V_w = \frac{\pi}{4} \frac{n_\Phi A_\Phi}{s} f_{yw} \cdot (D_e - 2c)
\end{aligned}
\tag{9}
$$

Unlike UCSD model, the coefficient (k) accounting for shear strength degradation due to ductility demand multiplies both the concrete and the transverse steel contributions; it varies linearly between 1.00 and 0.75 for $\mu_{\Delta pl} = (\mu - 1)$ between 0 and 5.

C617, 2009 (hereinafter referred to as "C617")

The Italian code [C617, 2009] suggests a formulation for the shear strength (V_{C617}) evaluation for RC bridge piers, given by the sum of concrete, transverse reinforcement, and axial compression contributions. Such a formulation is derived by the Original UCSD degrading model [Priestley et al., 1994], except than for the degrading coefficient (k), which varies linearly between 0.29 and 0.10 for

displacement ductility variable between 1.0 and 4.0, and the inclination (θ) - assumed as 45° (Eq. (10)). In Eq. (10) the internal lever arm is assumed as the diameter of the circular tie, as suggested also by EC8 model. This model has been validated based on experimental results of tests on only solid, rectangular and circular, columns.

$$\begin{aligned} V_{617} &= V_N + (k \cdot V_c) + V_w \\ V_N &= \frac{(D_e - x)}{2L_V} N \\ V_c &= \sqrt{f_c}(0.8A_c) \\ V_w &= \frac{n_\Phi A_\Phi}{s} f_{yw}(D_e - 2c) \end{aligned} \quad (10)$$

U.S. Federal Highway Administration, 2006 (hereinafter referred to as "FHWA")

The American guidelines for seismic retrofitting of bridges [FHWA, 2006] provides a formulation for the shear strength (V_{FHWA}) evaluation of RC bridges columns, based on the model by [Priestley et al., 1994]. The shear strength is given by the sum of the three contributions (concrete, transverse steel and axial load), as shown in Eq.s (11-12).

$$\begin{aligned} V_{FHWA} &= V_N + (k \cdot V_c) + V_w \\ V_N &= \frac{(D_e - x)}{2L_v} N \\ V_c &= \sqrt{f_c}\left(0.8A_c\right) \\ V_w &= \frac{\pi}{4}\frac{n_\Phi A_\Phi}{s} f_{yw}(D_e - 2c)\cot(\theta) \end{aligned} \quad (11)$$

$$\theta = \arctan\left(\max\left(\frac{1.6\rho_w 0.8A_c}{\rho_l A_c}; \frac{D_e - x}{L_v}\right)\right) \quad (12)$$

In this case, the shear crack inclination (θ) should be evaluated according to Eq. (12) and (ρ_w) is the transverse reinforcement ratio (with respect to the circular crown). The degradation coefficient (k) varies between 0.3 and 0.05 for increasing ductility demand but a clear prescription about the strength degradation model is missing.

1.2 Research significance

The above-reported review of the state-of-the-art shows that, unfortunately, few experimental studies exist in literature on specimens with ordinary concrete (medium-low compressive strength) and poor seismic reinforcement details, typical of existing bridge structures in Mediterranean area and Italy [STRIT RT D.1.2], in particular. Moreover, a considerable portion of the existing experimental tests have been performed by applying monotonic loading history, less representative of the structural response to seismic loads. Literature review also highlighted that very few shear strength models specific for the analysed - and widespread - structural typology exist in literature; whereas no code specifically addresses this issue.

In this framework, the present experimental study analyses the seismic response of RC existing bridge piers with hollow circular cross section, medium-low compressive strength, and a *single* external layer of longitudinal reinforcement and circular ties. Main goals of this experimental study are: *(i)* the evaluation of failure mode, peak load, deformation capacity and energy dissipation capacity of piers with different slenderness; *(ii)* the assessment of the deformability contributions due to flexure, shear and fixed-end-rotation mechanism to the overall applied top displacement; *(iii)* the collection of experimental tests from literature, similar to those tested herein, which exhibited a shear-critical behaviour; *(iv)* the evaluation of the capability of main shear strength models from literature or codes to predict experimental failure mode and shear strength for shear-critical piers.

To these aims, two reduced-scale hollow circular RC piers with different slenderness ratio have been realized and experimentally tested under cyclic lateral loading. The specimens have low values of longitudinal and transverse reinforcement ratios, and no adequate structural details or proper confinement requirements, as typical of design practices of Italian constructions before ‘80s. Two different failure modes were expected depending on the specimen aspect ratio.

Herein, first, specimens and experimental program details are described. Then, the global experimental lateral response, damage states evolutions and dissipated energy are investigated, and the main deformability contributions are experimentally evaluated. Finally, a focus on shear-critical piers have been performed, also collecting a proper experimental database of similar RC members

from literature that exhibited brittle failures. A comparison between the main shear strength capacity models from codes and literature and experimental results is carried out in order to select the model that provides the best numerical prediction.

2 EXPERIMENTAL CAMPAIGN

The tested specimens have been designed to be representative of typical existing piers of Italian bridges designed prior to 1980 (particularly, in terms of materials, geometry and reinforcement details). Therefore, the design process took into account the main outcomes of a deep analysis of a wide sample of Italian RC infrastructures [STRIT RT D.1.2] and provisions from literature [FIB 39, 2007], where different parameters are investigated (cross section shape, axial load ratio due to gravity loads, geometrical longitudinal and transverse reinforcement ratios, mean values of materials strength).

Most of existing Italian bridges have been constructed prior to 1980, before the advancement in earthquake engineering principles and seismic design codes [Cassese, 2017]. Walls and single piers represent the most widespread systems. Hollow cross section is the most adopted solution for RC bridge piers; other widespread solutions are solid circular and rectangular piers. Slenderness of piers - defined as the height to cross section depth ratio – is generally lower than 5.0; in particular, almost 50% of the analyzed piers presents slenderness values smaller than 2.5. Typical serviceability values of axial load ratio (v) range between 1% and 5%. Furthermore, common values for geometrical longitudinal reinforcement ratio are lower than 1%, while typical values of geometrical transverse steel reinforcement ratio range between 0.04% and 0.12%. Typical Italian bridge piers are generally characterized by poor concrete and relatively high strength steel. Mean values of concrete cylindrical compressive strength (f_c) vary from 10 MPa and 30 MPa; mean values of yielding strength (f_y) for steel range between 400 MPa and 550 MPa [Cassese, 2017; STRIT RT D.1.2].

As a result of this investigation, the bridge piers tested and presented herein were designed according to a non-seismic design, typical of the considered time-period, thus resulting in quite large ties spacing and 90° hooks, leading to lack of confinement, and poor concrete compressive strength. The resulting geometry and reinforcement details are described in the following (see Figure 1).

2.1 Description of the specimens and materials properties

The experimental program consists of two specimens, identified hereinafter as PC1 and PC2, representing two bridge piers with the same hollow circular cross section and reinforcement details, but different aspect ratio. The adopted scale factor is 1:4, for sake of convenience due to the capacity of the laboratory. The external diameter (D_e) is equal to 55 cm (corresponding to 220 cm in the full-scale) and the thickness (t_w) is 10 cm (corresponding to 40 cm in the full-scale). The geometrical longitudinal reinforcement ratio (ρ_l) is equal to 0.85%, provided by a single layer of rebars with a diameter (d_b) of 8 mm, placed along the external surface with a clear concrete cover depth (distance between the external fibre of the cross section and the outer surface of transverse bars) equal to 10 mm. The transverse reinforcement percentage (ρ_w) is equal to 0.06%, with d_b = 3 mm circular ties spaced at 120 mm and 90-degree end hooks. The tallest specimen (PC1) is 165 cm high; the shortest one (PC2) is 110 cm high. Consequently, the tested piers have aspect ratios (L_V/D_e) equal to 2.00 and 3.00 - for Test PC1 and PC2, respectively - in which L_V is the shear span of the pier (distance from the base of the pier to the loading point).

A poor-quality concrete has been used [STRIT RT D.1.2]. The mean value of cylindrical compressive strength (f_c) is equal to 15.6 MPa. Aggregates dimensions have been designed to be representative of those commonly adopted for ordinary concrete, on one hand, and properly scaled due to the reduced scale of the specimens in order to limit the size effect on the experimental results [Ohtaki, 2000]. The aggregates granulometry [Cassese, 2017] finally results compatible with the tight concrete cover.

Mean values of yielding strength (f_y) and ultimate strength (f_t) are equal to 540 MPa and 620 MPa, respectively, for longitudinal reinforcement. Mean values of yielding (f_{yw}) and ultimate strength (f_{tw}) of transverse reinforcement were equal to 655 MPa, and 690 MPa, respectively. Applied axial load ratio was equal to the 5%, representative of axial load ratios in service conditions for Italian bridge piers [STRIT RT D.1.2]. Main properties of the specimens and adopted materials are finally shown in Table 1 and Table 2.

2.2 Test setup and loading protocol

The tests have been performed by applying horizontal displacement cycles under quasi-static loading thanks to a hydraulic actuator acting as shown in Figure 2. The actuator-to-specimen connection reproduces a hinge. A rigid cap has been realized on the top of the piers in order to distribute axial and lateral loads on section flanges. The axial force is applied thanks to a closed system made up of *(i)* a hydraulic jack - located between the anchorage plate of the strands and the cap top surface, acting in load control, and *(ii)* three post-tensioned high-strength steel strands, fixed on the bottom side of the specimen by means of anchorage devices embedded in the pier foundation, and crossing the top of the specimen thanks to a full height hole in the cap. Four post-tensioned rebars restrain the foundation to the lab strong floor, thus avoiding any rotation or translation of the base during the test. Figure 2 shows a schematic view of the test setup described above. Hereinafter, the direction along which horizontal displacements are applied is referred to as east–west direction. Consequently, the perpendicular direction will be referred to as north-south direction. The system adopted to monitor global forces and displacements consists of two load cells, for horizontal and vertical forces, and a wire potentiometer fixed to an external point and connected to centreline of the pier cap (see Figure 2).

A proper monitoring setup was designed and adopted for both the specimens, aiming investigating about deformability contributions that characterize their response. In particular, on each specimen, a system of 14 Linear Potentiometers (LPs) was installed (4+4 on the two webs and 3+3 along the east/west directions), defining two "monitoring panels" as shown in Figure 3a. Note that only Monitoring Panel 1 (see Figure 3a) is present for the shortest pile (PC2). A system of aluminium tubes - properly connected to the specimen - sustains diagonal and vertical LPs to preserve the reliability of the local measures. The diagonal LPs ("LPd" in Figure 3a), were connected to the ends of these aluminium tubes, and the vertical LPs ("LPv" in Figure 3a) to central bolts (realized in the wall thickness along the loading direction). Flexural deformations and base rotation were measured by means of two vertical Linear Variable Displacement Transducers (LVDTs), placed diametrically

opposed along the loading direction, fixed at the pier-foundation interface ("LVDTb" in Figure 3a). Four additional horizontal LVDTs were installed as shown in Figure 3b for the squat specimen (PC2), in order to better monitor the width of shear cracks during the test, which are expected to be more significant due to the lower slenderness of this specimen.

Strain gauges (SGs) were also applied on the outermost couple of longitudinal rebars (along the loading direction) and on a couple of longitudinal rebars identified by a 45° inclined direction respect to the loading direction (see Figure 3c). These strain gauges were located just above the column base to monitor the development of steel strains. Finally, four cameras were installed along the four cardinal directions to monitor cracks evolution.

The testing procedure started applying axial load until 5% axial load ratio was reached. Then the specimens were subjected to quasi-static cycles of increasing horizontal displacement, under displacement control, with three push-pull cycles at displacements corresponding to the following peak drift (i.e. top displacement-to-shear span ratio) values: 0.25%, 0.50%, 0.75%, 1.00%, 2.00%, 3.00%, 4.00%, 5.00%, unless failure occurred earlier.

3 EXPERIMENTAL GLOBAL RESPONSE AND OBSERVED DAMAGE

Main global results are described and analysed in this section, in terms of lateral load-displacement response and evolution of observed damage with increasing imposed drift levels.

3.1 Test PC1

Figure 4 shows the lateral load versus drift response related to Test PC1. Push and pull experimental cycles appear symmetric during the whole test. The initial uncracked stiffness is equal to 67.7 kN/mm. At first cracking, the secant lateral stiffness becomes equal to 37.9 kN/mm. Such a reduction of stiffness corresponds to a lateral load of 29 kN, when first horizontal flexural cracks appear. Lateral stiffness decreases more considerably between 0.20% and 0.67% drift.

At lateral load values equal to 86.7 kN and -86.4 kN, respectively in push and pull directions, *first* yielding in longitudinal reinforcement is reached. This condition occurred for drift values equal

to +0.49% and -0.44%, in push and pull directions, respectively, when strain measures of longitudinal rebars provided by strain gauges - located at the base of the specimen - (see Figure 5) reach the yielding strain ($\varepsilon_{s,y}$ = 2.7‰). Beyond those values, SGs measures cannot be considered to be reliable. Note that experimental and theoretical values of *first* yielding appear very close each other. More in details, theoretical (V'_y) have been calculated by means of a section analysis performed in *OpenSees software* [McKenna, 2000], by using the material properties obtained from experimental tests on the adopted concrete and steel. [Mander et al, 1988]'s model is used for concrete (*Concrete04 uniaxial material* in *OpenSees*) and an elasto-plastic with hardening stress-strain relationship is adopted for steel (*ReinforcingSteel uniaxial material* in *OpenSees*). The section has been discretized in 16 rings × 16 wedges concrete fibers and 24 steel fibers (located as longitudinal reinforcement bars). As a result, theoretical (V'_y) value is equal to 86 kN for test PC1.

Peak load is reached at 1.91% drift for positive (push) loading direction and -1.87% drift for negative (pull) loading direction. The corresponding peak values of lateral load are +108.2 kN and -102.4 kN, respectively. After peak load was reached, the lateral load-drift response is basically governed by a flexural behaviour. As a matter of fact, post-peak phase is characterized by a strength gradual reduction due to the spalling of concrete cover and the buckling of longitudinal bars in compression near the base section. Such a strength degradation follows an almost linear branch described by a softening stiffness (calculated on the envelope of first cycles of loading steps V, VI and VII) equal to about -10% and -5% of the initial uncracked stiffness, in push and pull directions, respectively. The intra-cycle strength drop develops from 15% to 23% from the fifth to the seventh loading step. During the last push-pull cycle, at 4.90% drift, a series of sudden intra-cycle strength drops/stiffness drops are observed in both loading directions, corresponding to the failure of the outer longitudinal bars in tension due to oligo-cyclic fatigue caused by buckling/tension cycles. The test has been interrupted at the end of the eighth loading step (at 4.90% drift), when the strength reduction with respect to peak load - and evaluated on the backbone of the response - was equal to 40%, both in positive and negative directions (see Figure 4).

The damage evolution with the imposed drift level and the final damage state are reported in Figure 6 for this test and briefly described in Table 3. Horizontal hairline cracks appear on the west

and east faces orthogonally to the loading direction along the three stirrups closest to the base of the specimen during the first loading stages, namely at 0.20% drift (see Figure 6a). The second loading step (drift = 0.43%) is characterized by the spreading of flexural cracks along the specimen's height. First slight diagonal cracks appear on the north and south faces as extension of the flexural cracks for a drift of 0.67% (see Figure 6b), at 96.2 kN in positive direction and -96.4 kN in negative direction. For a drift value of 0.91%, existing cracks increase their width and further shear cracks develop as extensions of flexural cracks. It is interesting to highlight the pinching effect of the hysteretic loops (in Figure 4) starting from this cycles set, enhanced by the sudden increase in width of diagonal cracks (see Figure 6c). When a drift equal to 1.91% is reached, corresponding to the peak load, the damage at the base of the pier develops quickly: vertical cracks appear in concrete cover due to longitudinal bars buckling and concrete spalling is observed near to the base section (for negative loading direction), as showed in Figure 6d. In particular, at 2.92% drift a significant concrete spalling related to a more pronounced buckling of longitudinal bars - within the distance between the base and the first layer of transverse reinforcement occurs (see Figure 6e). The concrete cover spalling leads to a strength reduction with respect to the peak load (evaluated on the backbone of the response) of about 7% and 3% for positive and negative loading, respectively. During the seventh cycles set, for a drift of 3.91%, diagonal cracks considerably widen and concrete cover within the distance between the base and the first layer of transverse reinforcement is completely spalled off, except for a small central portion (see Figure 6f). This phenomenon is associated to an intra-cycle strength degradation equal to about 20% for both loading directions, as explained above. During the last cycles set (drift = 4.93%), concrete of the compressed flanges is completely crashed and concrete cover spalling spreads at second level of transverse reinforcement (see Figure 6g). Test PC1 fails in flexure. A picture of the final damage state at the base of the column is reported in Figure 6h.

Figure 6 and Table 3 also report the imposed ductility demand (μ_i') for each cycle (when displacement demand exceeds the first-yielding displacement), the latter computed as the ratio between the maximum imposed drift ratio (DR_i) in the i^{th} cycle and the mean value (between push and pull directions) of the first-yielding drift ratio (DR'_y).

The test was performed under constant axial load, as explained previously. Therefore, the evolution of the axial load bearing capacity of the pier during the test can be investigated by means of the vertical elongation of the hydraulic jack (Δ_a) located on the top of the pier, which represents an experimental measure of the shortening of the pier during the test (see Figure 7). If a sudden significant elongation of the hydraulic jack occurs, it is most likely due to the sudden reduction in axial stiffness of the pier, due to concrete cover spalling and buckling of longitudinal bars. Figure 7 shows that when very small lateral load levels are applied, the columns tend to elongate with increasing lateral deformations, as a result of crack opening along the column height. When the column experienced further damage, the tendency to elongate reversed into shortening which continues until the final (flexural) failure occurs. A quite significant increase in the hydraulic jack elongation occurs after yielding was reached. At V cycle, at peak load, the elongation of the hydraulic jack shows an increment of about 4 mm. Such an elongation further grows up to about 10 mm at flexural failure (VIII cycle). Hydraulic jack elongation increases progressively throughout the test, thus excluding the evidence of an eventual loss of axial load bearing capacity for test PC1.

3.2 Test PC2

The experimental lateral load versus drift response for Test PC2 is shown in Figure 8. The loading history actually applied consisted of five complete sets of three push/pull cycles and a last single push/pull cycle corresponding to a shear failure occurrence. Unlike the previous specimen, the experimental response of Test PC2 is characterized by a slight asymmetry during the push/pull cycles, in terms of lateral load. Such an evidence can be ascribed to the cyclic evolution of the test and the development of the shear cracks. As a matter of fact, first shear cracks appear for a given loading direction, and, then, when the loading direction changes, such cracks can only partially close, thus leading to a lower value of the maximum achieved lateral load, and - for a given imposed drift level - a lower value of the lateral stiffness [Cassese et al., 2017].

Test PC2 exhibits an initial uncracked stiffness equal to 206.8 kN/mm and, after first cracks, a secant lateral stiffness at first cracking of 133.8 kN/mm. Such stiffness reduction corresponds to a lateral load of 45 kN, when first flexural cracks appear. A more significant reduction is observed for a

drift value ranging between 0.16% and 0.60%, when first shear cracks also appear. During the third loading step, for lateral load values equal to 138.0 kN and -133.6 kN, respectively in push and pull directions, the specimen reaches the *first* yielding condition. More in details, this *first* yielding state is reached when longitudinal bars strain measures provided by strain gauges located at the base of the specimen (see Figure 9) exceeded the yielding strain ($\varepsilon_{s,y}$ = 2.7‰) both in push and pull loading directions, for drift values of 0.49% and - 0.52% respectively. Also for this test, SGs measures are reported in Figure 9 up to values considered as reliable. Also in this case the experimental and theoretical values of *first* yielding appear very close each other. Theoretical (V'_y) value – calculated like to test PC1 – is equal to 129 kN.

Peak load is reached at +1.78% drift for positive loading direction (push) and -1.80% drift for negative loading direction (pull). The corresponding peak values of lateral load are +167 kN and -147 kN, respectively. The intra-cycle strength drop – developed at peak load drift level – reached 15%. Test PC2 has been stopped at the end of the pushing phase of the first cycle at 2.87% drift. In fact, during pushing phase, for a drift value of +2.49%, a significant drop in strength - equal to 72% - is observed, from +149 kN to +42 kN at a drift value of +2.87%. Such a drop is due to the sudden and significant widening of the main shear cracks developed before. At the end of the test, the strength reduction with respect to the peak load (and evaluated on the backbone of the response) is equal to 75%.

The damage evolution with the applied drift level and the final damage state for Test PC2 are reported in Figure 10 and summarized in Table 4. In particular, first hairline cracks appeared on the west and east faces along the first three stirrups during first loading cycles, namely at 0.16% drift (see Figure 10a). The second loading step (drift = 0.37%) was characterized by the spreading of flexural cracks and the occurrence of first diagonal cracks as extension of the flexural ones toward the compressed zone (see Figure 10b). More significant diagonal cracks appear on the north and south faces for a drift level of 0.60% (at 146 kN in positive direction and -137 kN in negative direction). In particular, a couple of diagonal cracks occurs from the top corner to the opposite down corner with an inclination angle of about 42 degrees with respect to the horizontal direction (see Figure 10c).

At 0.83% drift, existing shear cracks increase their width, particularly two principal ones, and further shear cracks are observed in the central part of the specimen (see Figure 10d). When a drift value equal to 1.82% is applied, corresponding to the peak load condition, damage at the base of the pier develops quickly: vertical cracks appear in concrete cover due to the longitudinal bars buckling and the concrete cover spalling observed in a small portion near to base section along the east/west direction (see Figure 10e). During the subsequent pushing phase, for a drift value of +2.49%, the main shear crack opens suddenly up to a width of about 13 mm, along an ideal concrete strut with a medium inclination angle of about 42 degrees, as observed before (see Figure 10f). Consequently, shear sliding between the upper and the lower part of the specimen is observed, causing the failure in tension of the circular ties along the main diagonal crack and the flexural deformation of the involved dowel bars (see Figure 10g). Test PC2 fails in shear after flexural yielding. A picture of the final damage state is reported in Figure 10h.

In Figure 10 and Table 4, the imposed ductility demand (μ_i') – defined above – is also shown for each cycle when displacement demand exceeds the first yielding displacement.

As mentioned above, during the pushing phase at +2.49% drift, the main diagonal crack suddenly increases its width. Such a phenomenon has been directly monitored by means of the LVDTs system shown in Figure 3b. Figure 11 shows the algebraic sum (Δ_H) between two diametrically opposed horizontal LVDTs for each level, useful to analyse the horizontal component of the shear cracks width evolution during the test. It can be noted that up to the third loading step (drift = 0.60%), the width of diagonal cracks is almost negligible and only some diagonal cracks near to the base section (level 1) are present. The fifth loading step (at 1.82% drift) is characterized by an almost linear increasing of the shear cracks width, on the central part of the specimen (from about 0.5 mm to about 4 mm). During the subsequent pushing phase, at +2.49% drift, a sudden increase in cracks width can be observed, corresponding to the widening of the main shear crack up to about 13 mm. Moreover, the main shear crack is wider in the lower part (level 1) with respect to upper one (level 2). Thus, it seems that the failure mechanism has been characterized by a slight rotation as well as a horizontal sliding only.

Also for this test, the evolution of the axial load bearing capacity of the pier during the test can be investigated. The vertical elongation of the hydraulic jack located on the top of the pier, is shown in Figure 12. The trend of such an elongation appears quite similar to test PC1 (compare to Figure 7). A quite significant increase in the hydraulic jack elongation is observed after yielding occurred and first shear cracks appeared. At V cycle, when peak load is reached, the elongation of the hydraulic jack suddenly increases of about 4 mm. Such an elongation further increases up to about 4.8 mm after shear failure (VI cycle), when the test was interrupted due to the very significant later load reduction (-75%). Also for this test, the hydraulic jack elongation increases progressively throughout the test. No sudden significant elongation of the hydraulic jack occurs up to the last step of the test, thus excluding the evidence of an eventual loss of axial load bearing capacity for test PC2. Furthermore, previous experimental studies from literature have shown that loss of gravity load bearing capacity after shear failure tends to occur when the shear strength degrades to approximately zero [Yoshimura and Yamanaka, 2000; Elwood and Moehle, 2004]. Therefore, data available from test PC2 after shear failure are not sufficient to experimentally detect an axial load failure. The latter could be eventually extrapolated and associated to the final point on the idealized backbone of test PC2 up to zero shear strength [Elwood and Moehle, 2004].

3.3 Comparison of global response

Lateral load-drift responses of the tested specimens are compared in Figure 13 in terms of envelopes corresponding to the first sub-cycles for each loading step. Table 5 reports experimental values of lateral loads and drift ratios at *first* yielding ($V'^{(+)}_y$, $V'^{(-)}_y$, $DR'^{(+)}_y$, $DR'^{(-)}_y$), at peak load ($V^{(+)}_{max}$, $V^{(-)}_{max}$, $DR^{(+)}_{max}$, $DR^{(-)}_{max}$), and at "ultimate" condition ($DR^{(+)}_u$, $DR^{(-)}_u$) for both loading directions. In particular, the 20% strength reduction on the experimental backbones – with respect to the peak load – identifies the achievement of the "ultimate" condition. Table 5 also shows the experimental failure modes (FMs): flexure (F) mode for Test PC1, and shear failure after flexural yielding (FS) mode for Test PC2.

Rather surprisingly, experimental values of drift ratios at yielding for test PC1 and PC2 are quite similar each other. Actually, the pier PC2 was characterized by a significant shear diagonal cracking

pattern at yielding condition (see damage state at cycle III in Figure 10), unlike test PC1. Therefore, the flexural deformability contribution to yielding drift ratio for test PC2 is affected by the tension shift due to diagonal cracking, in addition to the "pure" flexural deformability contribution, unlike test PC1. As expected, given the drift level, the lower the slenderness, the higher the lateral load. The deformation capacity (DR_u) is lower for the squat specimen (PC2).

3.3.1 Energy dissipation and equivalent viscous damping

A comparison between the two specimens can be performed also in terms of energy dissipation capacity. The dissipated energy for the specimens PC1 and PC2 - calculated as the area underneath the experimental lateral load-displacement curve - is shown in Figure 14. In particular, Figure 14a and Figure 14b show the Cumulative Dissipated Energy (CDE) and the energy dissipated in each cycle ($E_{h,i}$), namely the area within one complete cycle of the force-displacement response, respectively, depending on the applied drift.

At first glance, given the imposed drift value, the evolution of the dissipated energy for the two specimens appears quite similar up to 2.87% drift, when shear failure occurred to specimen PC2. The shear failure occurrence for low levels of drift demand limited the displacement capacity of test PC2, as already shown in the previous section. This is confirmed also in terms of energy, as expected, leading to a lower total hysteretic energy dissipation capacity for test PC2 - equal to about 32% of test PC1 (both evaluated at the end of the test).

About the dissipated energy for each cycle, for a drift level of about 2.00%, the CDE characterizing the test PC2 is 16% lower than the corresponding one for test PC1 despite the higher value of lateral load reached by test PC2. This effect can be mainly ascribable to the shear failure onset for the squat specimen. A significant CDE drop (about 42%) at 1.82% drift characterizes test PC2. Such a drop is mainly due to the sudden development of shear cracks and the reduction of the other more dissipative mechanisms. Finally, for Test PC1, the dissipated cyclic energy is characterized by a significant increase since the fourth cycle (drift = 0.91%), when the element overcomes the linear field of behaviour (yielding of longitudinal bars steel was reached in the previous cycle).

As known, the dissipated energy (DE) depends on the maximum achieved load and displacement at each cycle. Therefore, the equivalent damping ratio (ξ_{eq}), often adopted in literature as a measure of the specific DE [Priestley, 2007], can be calculated in order to perform a clearer comparison between specimens PC1 and PC2. In particular, the experimental equivalent damping at the i^{th} cycle ($\xi_{eq,i}$) is calculated as a function of the dissipated energy $E_{h,i}$, according to Eq. (13):

$$\xi_{eq,i} = \frac{1}{2\pi} \cdot \frac{E_{h,i}}{\bar{V}_i \cdot \bar{\Delta}_i} \tag{13}$$

where, ($\bar{V}_i$) and ($\bar{\Delta}_i$) are the averaged values between positive and negative loading directions of maximum lateral load and top displacement, respectively, at the i^{th} cycle. Generally, in literature (ξ_{eq}) is expressed as a function of the displacement ductility (μ) through the functional form reported in Eq. (14):

$$\xi_{eq} = \xi_0 + a \cdot \left(1 - \frac{1}{\mu^b}\right) \tag{14}$$

where (ξ_0) is the initial viscous damping (usually 5% for RC structures), (a) and (b) are the hysteretic model coefficients [Priestley, 2003].

In Figure 15, the experimental equivalent damping is reported for both the specimens, together with the prediction curve by [Priestley, 2003] for concrete columns (based on the modified Takeda hysteresis rule), and the experimental best-fit curve, obtained by assuming the functional form in Eq. (14) and by imposing ξ_0 = 5%. In particular, herein, for each specimen, the equivalent damping is computed as a function of the displacement ductility (μ), defined as the ratio between the maximum imposed displacement in each cycle and the yielding displacement. The latter is not exactly the displacement corresponding to the *first* yielding; it is obtained through a bi-linearization of the experimental envelope - as shown later in section 5 (see Figure 18a) - in tune with the proposal by [Priestley, 2003; Priestely et al., 2007] and [Ranzo and Priestely, 2001] (finally resulting equal to 9.0 mm and 6.7 mm, for test PC1 and PC2, respectively). Then, a non-linear least square regression is

performed to obtain the best-fit to the experimental results for the parameters (a) and (b), assuming the functional form reported in Eq. (14) with initial damping $\xi_0 = 5\%$.

Equivalent viscous damping is generally higher for test PC1, as expected, and increases with increasing ductility, except than for the last ductility demand level reached by test PC1, likely due to the onset of degrading flexural mechanisms also for test PC1 at such drift level. In fact, as explained in detail in section 3.1, after the peak load, a pronounced softening in the global response can be observed (due to concrete crushing, bars buckling, diagonal cracks, and so on), up to the strength/stiffness drop due to the failure of the outer longitudinal bars in tension during the last cycle.

The experimental fitting shows a steeper increasing trend of the equivalent viscous damping for lower ductility values, whereas for higher ductility level ($\mu > 3$) the trend becomes almost constant. This can be interpreted with a lower energy dissipation capacity of existing hollow circular columns with respect to that predicted by adopting the "thin" Takeda model hypothesis for large ductility demand. The reason of this unexpected result can be found in the considerable degradation of the dissipation mechanisms also for the ductile test PC1, as described above.

4 EXPERIMENTAL DEFORMABILITY CONTRIBUTIONS

The overall top displacement (Δ) of each specimen is due to the sum of three deformation mechanisms: flexure (Δ_f), shear deformation (Δ_s) and fixed-end-rotation due to longitudinal bar slip at column base (Δ_θ). Past experimental campaigns [e.g., Delgado, 2009; Cassese et al., 2017] showed that the seismic response of RC elements with hollow cross sections can be characterized by a significant flexure-shear interaction, depending on their aspect ratio. For such elements, deformability contribution due to shear mechanism might represent an important portion of the global deformability and, therefore, it is analysed in this section.

As already described in section 2, a proper monitoring system was installed on the specimens to measure all the above-mentioned deformability contributions. In particular, (Δ_f) and (Δ_s) are evaluated under the hypotheses of *(i)* uniform curvature distribution along each "monitoring panel", and *(ii)* small angles and uniform shear deformation over each "monitoring panel" height [see Cassese et al.,

2017]. On the other hand, (Δ_θ) is caused by the slippage of reinforcing bars from the foundation and it cannot be directly evaluated. Instead, the base rotation (θ_b, including also flexural deformation at the base zone) can be measured by means of the "LVDTb". The related top displacement (Δ_b) can be calculated as the product between (θ_b) and the corresponding distance between the base and the top of the pier.

Figure 16 shows the deformability contributions to the overall top displacement depending on the drift level. Plots are shown until displacement measures from LVDTs and LPs can be considered reliable. Measures corresponding to the first cycles for each drift level are shown, considering the average values between the two loading directions. For Test PC1, damage state evolution lead to the detachment of some instruments located at the base, and, thus, for this specimen, the plot in Figure 16a is interrupted when peak load was achieved. Vice-versa, for Test PC2, all the measures are considered reliable up to the last imposed drift level (see Figure 16b). Figure 16 shows that, for both tests, the flexural deformability contribution (which should be considered as the sum between Δ_b and Δ_f) is more important than the deformability contribution (Δ_s), nevertheless the latter cannot be considered negligible, especially for the squat specimen PC2, as expected. Furthermore, for the slenderest specimen (Test PC1), the shear contribution is almost constant and very low, namely, (Δ_s/Δ) is equal to about 5.7% up to 0.91% drift. At peak load condition (drift = 1.91%), the increase of existing diagonal cracks width leads to a shear contribution to the top displacement equal to about 10%, which is the maximum value measured during Test PC1. Test PC2 is characterized by a shear contribution that is higher than 10% since the second cycle (drift = 0.37%), when (Δ_s/Δ) already reaches a value of 11.0%. Test PC2 exhibits a growing trend of the shear deformability contribution with the applied drift level. As a matter of fact, (Δ_s/Δ) ratio reaches an average value of 15.3% at yielding cycle and 25.4% at shear failure.

It should be also noted that for Test PC2, the deformability contribution (Δ_b/Δ) increases after flexural yielding of about 10% respect to the previous drift level, together with shear contribution (Δ_s/Δ). This is mainly due to the development of significant diagonal cracks and flexural damages concentrated at the base of the specimen after yielding. On the other side, for Test PC1, (Δ_b/Δ) is about constant during the test, likely because flexural cracks are distributed along the specimen height.

Finally, in Figure 17 the evolution of (Δ_s/Δ) with the applied drift level can be observed for both the tests: the lower the aspect ratio, the higher the deformability contribution due to shear mechanism, as expected.

Note that, unlike for the experimental flexural deformations, the evaluation of shear deformation is less homogenous between studies from literature [Beyer et al., 2011]. In particular, the approach adopted herein is strictly rigorous only if the curvature is constant along each monitoring panel. Under this hypothesis, any difference in the LVDTs diagonals length can be attributed to shear deformability only. Otherwise, a portion of such difference is due to the flexural deformations. A more rigorous approach to evaluate the shear deformability contribution was proposed by [Hiraishi, 1984] to explicitly consider this issue. The application of such an approach to tests PC1 and PC2 modifies only slightly, on average, the deformability contributions presented in Figure 16. In particular, observed variation – with respect to the approach adopted in Figure 16 – for test PC1 ranges from 0% (before yielding) to -20% (just after yielding); mean variation (considering all the applied drift levels) is equal to -6%. Similar variations are observed for the shortest pier (PC2), ranging between 0% and -16% (just after yielding); mean variation (considering all the applied drift levels) is equal to -6%.

5 SHEAR FAILURE ASSESSMENT

A thorough investigation about the predictive capability of the main shear capacity models applied to members with hollow circular cross section is carried out in this section. To this aim, a proper database of tests available in literature on shear-critical existing hollow circular RC elements has been collected and analysed (section 5.1). Then, in section 5.2, all the models described in section 1.1.2 are applied to the collected database and the results of these experimental-versus-predicted comparisons are analysed**.**

5.1 Experimental database

A proper database of experimental tests from literature among those presented in section 1.1.1 – similar to piers tested by the Authors – on shear-critical piers with hollow circular cross section has

been collected, including experimental Test PC2, described in section 3. This database includes 13 tests, representing the experimental state-of-the-art about non-conforming RC columns with hollow circular cross section exhibiting a shear failure (with or without flexural yielding). Note that, tests by [Kishida et al., 1998] and [Völgyi et al., 2014a] are not included in the collected database because related to specimens with high-strength concrete, characterized by different shear resistant mechanisms [Collins and Kuchma, 1999] and not representative of the most of (low-standard) existing bridge piers. Among the considered specimens, some units were tested under unidirectional cyclic lateral loading in single curvature [Ranzo and Priesltey, 2001; Yeh et al., 2001; Cheng et al., 2003] with fixed-end at the bottom (cantilever scheme). Some others [Regis, 1990; Turmo, 2009] were tested as simply supported beams on mechanical hinges, under unidirectional monotonic transverse load applied at mid-span. All the specimens are characterized by uniform longitudinal and transverse details throughout the length. Finally, two tests are characterized by the absence of transverse reinforcement; whereas for some others no axial load was applied. The ranges of variability for the main geometrical and mechanical properties of the collected tests are summarized in Table 6.

The experimental force-displacement responses of these tests are collected and analysed. The backbone curve of the global response is defined for each test. The main characteristic values of lateral force *V* and drift ratio *DR* are identified, as explained in the following. All the collected tests exhibited a shear failure, with or without flexural yielding. Herein, a uniform FM classification is applied, based on the values of theoretical *first* yielding load (V'_y). As already expressed in section 3.1, theoretical *first* yielding load (V'_y), have been calculated by means of a section analysis performed in *OpenSees software* [McKenna, 2000], by using [Mander et al, 1988]'s model for concrete (*Concrete04 uniaxial material* in *OpenSees*) and an elasto-plastic with hardening stress-strain relationship for steel (*ReinforcingSteel uniaxial material* in *OpenSees*).

Since all the collected tests exhibited a shear failure, when the peak load (V_{test}) is lower than load at *first* yielding (V'_y), a shear (S) failure mode is assumed to occur; otherwise, flexure-shear (FS) failure mode is assumed. Consequently, all the monotonic tests (M) result classified as S-failure and all the cyclic tests (C) result FS-failure tests.

For the FS-failure mode, it is necessary to evaluate the ductility demand, in order to account for shear strength degradation. This is not the case for monotonic tests, for which no cyclic strength degradation develops. Therefore, particularly for cyclic tests, (μ_{test}) is defined as the ductility demand at the peak load point; whereas (μ_s) is the ductility demand at the 20% strength reduction point after peak load – or at the maximum-recorded displacement when lateral load does not reach the 20% strength reduction (as in [Elwood, 2004]). It is crucial to distinguish between these two values of displacement ductility demand, depending on the shear capacity model adopted, as discussed in detail in the next section. Note also that (μ_{test}) and (μ_s) are calculated by considering the loading direction where shear failure occurred.

In summary, Table 7 shows main properties (geometry, reinforcement details, material properties, and axial load ratio), shear strength (V_{test}), theoretical *first* yielding load (V'_y), and failure modes (FM_{exp}), for all the specimens included in the collected database.

5.2 Shear strength assessment

All the models described in section 1.1.2 have been applied to the specimens belonging to the collected database in order to evaluate their efficiency, by considering the experimental failure mode for shear strength prediction. Some details should be explained in order to understand the implementation of such models carried out herein (see Table 8).

First, note that for all the formulations proposed by codes, mean values of materials strength and unitary values for the reducing factors, if any, are adopted for comparisons with experimental results.

"JH" model [Jensen and Hoang, 2010] is applied only to monotonic tests, since such a model is not able to take into account an eventual strength degradation due to cyclic loading. "FHWA" model also is applied only to monotonic tests, since a clear prescription about the strength degradation model is not provided, as highlighted in section 1.1.2; therefore, V_{test} is compared with the maximum predicted shear strength for this model.

Furthermore, in order to evaluate a shear strength value, the proposal by [Turmo et al., 2009], which only provides the shear strength contribution related to the transverse reinforcement, has to be combined with other approaches taking into account the remaining contributions due to concrete and

axial compression (if any) properly for the investigated elements. Therefore, herein, Eq. (7) will be adopted to compute the transverse reinforcement contribution (V_w) within the model by [Ranzo and Priestley, 2001]. The shear strength value evaluated in this way will be identified as (V_{RP+T}), hereinafter, and the resulting combination as "RP+T" model. Nevertheless, it is worth noting that "RP" model - in agreement with [Kowalsky and Priestley, 2000] - is based on the assumption that the shear reinforcement is active only along the shear crack in the flexural tension zone. On the contrary, [Turmo et al., 2009] – in its original version – assumes that transverse reinforcement is active along a hypothetical shear crack crossing the entire height of the element. These two approaches become more coherent – as suggested by [Turmo et al., 2009] – by assuming that the internal level arm *z* in Eq. (7) is equal to the difference (D_e – c – x), as in [Ranzo and Priestly, 2001]. In the application of "T" model, also the same angle θ proposed by "RP" model (30°) is assumed herein.

Moreover, for degrading shear strength models, a further specification is needed about the definition of displacement ductility demand affecting shear strength. In particular, (μ_{test}) is adopted to calculate (concrete) shear strength degradation related to the models by [Ranzo and Priestely, 2001] and Italian code [C617, 2009] (both deeply influenced by the model proposed by [Kowalsky and Priestely, 2000]). On the other hand, (μ_s) is used to calculate the (concrete+steel) shear strength degradation related to the EC8 model [Biskinis et al., 2004]. In addition, the yielding displacements underlying the calculation of these two kinds of displacement ductility demand are *nominal* yielding displacements, evaluated coherently with the proposal of each of the applied strength model, as explained in the following.

The yielding displacement (or equivalently the yielding drift, DR_y) underlying the calculation of (μ_{test}) – to be used in "RP" model (and consequently in C617 and "RP+T" models) – comes from a bi-linearization of the force-displacement envelope proposed by [Rando and Priestely, 2001], and also adopted in [Priestely, 2003] and [Priestley et al., 2007]. Such a bi-linearization is graphically shown in Figure 18a. In particular, drift ratio at this *nominal* yielding (DR_y) is defined as a function of first yielding drift ratio (DR'_y). (DR_y) and, consequently, (μ_{test}) are calculated as shown in Eq. (15):

$$DR_y = DR'_y \frac{M_n}{M'_y} \rightarrow \mu_{test} = \frac{DR_{test}}{DR_y} = \frac{DR_{test}}{DR'_y} \frac{M'_y}{M_n} \quad (15)$$

where (M_n) is the nominal flexural capacity calculated as suggested in [Priestley et al., 2007] - namely related to achievement of 0.4% strain in the most compressive concrete fiber, and ($M'_y = V'_y \cdot L_v$) is the first yielding moment related to the yielding of the outer longitudinal reinforcement bars.

On the other hand, the yielding displacement underlying the calculation of (μ_s) – to be used in EC8 model – comes from a (different) bi-linearization of the force-displacement envelope in tune with the proposal by [Biskinis et al., 2004] (see Figure 18b). Therefore, this yielding drift is calculated starting from the formulation proposed by [Panagiotakos and Fardis, 2001] for the chord rotation at yielding ($\theta_{y,P\&F}$). In summary, drift ratio at this *nominal* yielding, and, consequently, (μ_s) are calculated as shown in Eq. (16):

$$DR_y = \theta_{y,P\&F} \rightarrow \mu_s = \frac{DR_s}{DR_y} = \frac{DR_s}{\theta_{y,P\&F}} \quad (16)$$

It should be noted that the second definition of (DR_y) – adopted to implement the model by EC8 - is totally theoretical, namely not based on experimental data, unlike the approach adopted to calculate (μ_{test}). As a result, a further approximation error for EC8-3 model is inevitably introduced.

5.2.1 Results and discussion

Based on the remarks reported above, Figure 19 and Table 9 show the results of experimental-versus-predicted comparisons in terms of predicted-to-experimental shear strength ratio (V_{pred}/V_{test}). Red and blue colours are related to monotonic and cyclic tests, respectively. Dotted lines in Figure 19 are related to the mean values of (V_{pred}/V_{test}) and, in particular, black line represents the mean ratio considering together all the specimens.

It can be noted that models from literature considered herein generally underestimate the non-degraded shear strength (see monotonic tests), whereas models from codes overestimate the shear strength for such tests from +8% (C617) to +47% (EC8). On the other hand, models from codes slightly underestimate the degraded shear strength due to cyclic loading (from -9% to -4%), showing

quite high coefficients of variation (from 21% to 28%). Model by EC8 and FHWA provide the highest errors – especially for monotonic tests.

On average, the worst model appears the EC8 model both in terms of mean error (+27%) and COV (40%). This outcome is ascribable to the evidence that EC8 provides an empirical-based formulation for RC members [Biskinis et al., 2004] calibrated on an experimental database not considering hollow circular members at all. American guidelines [FHWA, 2006] systematically overestimate (+26%) the experimental shear strength (for monotonic tests to which it is applied), likely because no specific attention to the effective concrete shear strength contribution has been paid for hollow circular columns, and (V_w) contributions always higher than those related to "RP" model are obtained for the collected tests. On the other hand, the [C617, 2009] proposal results the best model among models by codes: on average its error is only +2% (with COV=19%).

"JH" model is a non-degrading shear strength model and it provides a systematic underestimation of the experimental shear strength (-19%). Actually this model has been validated on the basis of a database mainly made up of tests with high concrete strength [Kishida et al., 1998], which generally exhibit a reduced aggregate interlock contribution to the concrete mechanism component of the shear strength [Collins and Kuchma, 1999], thus justifying the observed outcome.

Model proposed by [Ranzo and Priestely, 2001] provides a mean (V_{pred}/V_{test}) ratio equal to -9% (and COV=17%), and offers a very good prediction of cyclic (FS) tests (mean V_{pred}/V_{test} is equal to 1.00 in this case). Note that "RP" model overestimates shear strength related to the same tests based on which it was validated (HS2, HS3). This error drastically reduces if the contribution of axial load (V_N) is totally neglected for these two tests. Therefore, [Ranzo and Priestely, 2001] suggested to neglect the V_N contribution, especially for the design of hollow circular RC piers. Nevertheless, if such a prescription (V_N=0) was applied to all the collected tests, the mean prediction error increases up to -23%. Therefore, it can be concluded that the contribution V_c+V_N by "RP" model should still be improved. This outcome is confirmed if tests PA1 and PA2 by [Regis, 1990] – without stirrups – are compared with V_{RP}.

Finally, if "RP+T" model is adopted, shear strength of tests with helicoidal stirrups are overestimated (+37% on average). Vice-versa, for the other tests, "RP+T" model generally slightly

underestimates shear strength, especially for S-failure tests (-9%, on average). Mean value of (V_{pred}/V_{test}) ratio results equal to 1.00 for "RP+T" model (with a COV equal to 19%), if all tests are considering together.

Table 9 also shows the predicted failure mode according to the adopted shear strength models. The predicted FM is evaluated by means of a comparison between the predicted non-degraded ($V_{R,max}$) and totally degraded ($V_{R,min}$) values of the shear strength and the lateral load corresponding to first yielding (V'_y) and peak experimental load (V_{test}). If ($V_{pred}=V_{R,max}$) is lower than (V'_y), a S-failure is predicted; on the opposite side, when ($V_{pred}=V_{R,min}$) is higher than ($V_{test} > V'_y$), a flexural (F) failure is predicted. Otherwise, the predicted failure mode is a FS-mode.

For cyclic tests, it can be observed that models are quite similar each other in FM prediction: in particular, "RP" and C617 models well predict the observed FM in 4/5 cases; whereas "RP+T" and EC8 models provide a good prediction of FM in 3/5 cases.

In summary, model by [Ranzo and Priestley, 2001] can be considered as a good choice to estimate shear capacity of existing bridge piers with hollow circular section, thanks to its prediction capacity in terms of *(i)* expected failure mode and *(ii)* predicted shear strength, especially for cyclic tests. On the other hand, the integration of "RP" model with the proposal by [Turmo et al., 2009] for (V_w) – slightly modified as explained previously – seems to provide promising results. Certainly, more data about similar specimens from future experimental campaign are necessary since they could be very helpful to support or confirm the trends observed and explained above or to support the proposal of a more comprehensive shear strength model, where all the shear strength contributions are specifically calibrated on columns with hollow circular sections.

6 CONCLUSIONS

The present work provides a contribution towards a deeper investigation about the cyclic lateral response of RC existing bridge piers with hollow circular cross section. In particular, two reduced-scale hollow circular RC piers different for aspect ratio have been tested under cyclic loading and constant axial load. The specimens were characterized by low percentage of longitudinal and transverse reinforcement (distributed on a single layer), with poor concrete, inadequate details and

lack of suitable confinement reinforcement. Such specimens represent a structural typology that is widespread worldwide, even if a very small number of related experimental tests has been found from literature. Two distinct failure modes were experimentally observed, depending on the specimen slenderness, namely, a flexure mode for the tallest piers and a flexure-shear for the shortest one.

Global response and the evolution of damage has been analysed and described in details for both the specimens. It was noted that lateral strength increases as the aspect ratio decreases, as expected. On the other hand, the lower the pier aspect ratio, the lower its ultimate deformation capacity. The squat specimen, which exhibited a flexure-shear failure mode, exhibited the lower value of ultimate drift. Local response in terms of deformability contributions due to flexure, shear and fixed-end-rotation mechanisms has been also investigated. For both tests, the flexural deformability contribution resulted as predominant with respect to the shear deformability contribution, nevertheless the latter cannot be considered negligible, especially for the squat specimen.

Finally, a focus on hollow circular shear-critical piers have been performed, collecting a proper experimental database of similar existing RC piers from literature that exhibited shear failures. Very few shear strength models specific for these RC elements exist in literature, whereas no code specifically addresses this issue, actually failing to recognise the distinctive features of this structural typology with respect to ordinary solid members. A comparison between the main shear strength capacity models from codes and literature and experimental results was carried out. It was observed that the Italian code [C617/2009] proposal results the best model among models by codes considered herein. Among models from literature, model by [Ranzo and Priestley, 2001] can be considered as a good choice to estimate shear capacity of existing bridge piers with hollow circular section, thanks to its prediction capacity in terms of both expected failure mode and predicted shear strength, especially for cyclic tests. On the other hand, the integration of model by [Ranzo and Priestley, 2001] with the proposal by [Turmo et al., 2009] for transverse reinforcement contribution – slightly modified in shear cracks angle and internal level arm calculations – seems to provide promising results. Certainly more data about similar specimens from future experimental campaign are necessary since they could be very helpful to support or confirm the trends observed and explained above or to support the proposal

of a more comprehensive shear strength model, in which all the shear strength contributions are specifically calibrated on columns with hollow circular sections.

List of notations

A_c cross section area (gross area without void)
A_e effective shear area
A_l total area of longitudinal reinforcement
A_Φ area of a single hoop or spiral
c concrete cover
C factor taking into account the discrete spacing of the hoops
d_b diameter of a single steel bar
D_e external diameter of the cross section
f_c concrete cylindrical compressive strength
f_{tef} concrete effective tensile strength
f_y yielding stress of longitudinal steel reinforcement
k coefficient of shear strength degradation
μ ductility demand
f_{yw} yielding stress of transverse steel reinforcement
L_V shear span
m longitudinal projection of the critical diagonal crack
N axial load
n_Φ number of active legs in the cross-section
p pitch of the continuous spiral
R′ radius of the circular or helical transverse reinforcement
s spacing of the transverse reinforcement
t_w thickness of the concrete ring
x neutral axis depth
z lever arm
α coefficient accounting for the column aspect ratio
β coefficient accounting for longitudinal steel ratio
γ ratio between void and external diameter
λ efficiency factor for transverse reinforcement in longitudinal direction
ν_o concrete effectiveness factor (plastic theory)
ν_s effectiveness factor for the reduction of the cohesion due to sliding crack
θ angle between the critical diagonal crack and the longitudinal axis
ρ_l geometrical longitudinal reinforcement ratio
ρ_w geometrical transverse reinforcement ratio
χ efficiency factor for transverse reinforcement in transversal direction

Acknowledgements

This work was developed under the financial support of STRESS S.c.a.r.l. STRIT Project "PON Ricerca e Competitività 2007-2013 and "ReLUIS-DPC 2014-2018 PR 2- Linea Strutture in cemento armato", funded by the Italian Department of Civil Protection (DPC). These supports are gratefully acknowledged.

REFERENCES

Aschheim, M., Moehle, J. P. [1992] "Shear strength and deformability of RC bridge columns subjected to inelastic cyclic displacements", Rep. No. UCB/EERC-92/04, Earthquake Engineering Research Centre, University of California at Berkeley, Berkeley.

Beyer, K., Dazio, A., & Priestley, N. (2011). Shear deformations of slender reinforced concrete walls under seismic loading. ACI Structural Journal, 108 (epfl-article-162084), 167-177.

Biskinis, D.E., Roupakias, G. K., Fardis, M. N. [2004] « Degradation of shear strength of rein-forced concrete members with inelastic cyclic displacement", ACI Structural Journal 101(6),773–83.

Calvi, G. M., Pavese, A., Rasulo, A., Bolognini, D. [2005] "Experimental and numerical studies on the seismic response of RC hollow bridge piers". Bulletin of Earthquake Engineering 3(3), 267-297.

Cassese, P., Ricci, P., Verderame, G. M. [2017] "Experimental study on the seismic performance of existing reinforced concrete bridge piers with hollow rectangular section", Engineering Structures 144, 88-106.

Cassese P. (2017). Seismic performance of existing hollow reinforced concrete bridge columns, PhD. Thesis, University of Naples Federico II, Italy, 2017.

CEN 2005. European Standard EN 1998-3: 2005 Eurocode 8: Design of structures for earthquake resistance. Part 3: Assessment and retrofitting of buildings. European Committee for Standardization, Brussels, 2005.

Cheng, C. T., Yang, J. C., Yeh, Y. K, Chen, S. E. [2003] "Seismic performance of repaired hollow-bridge piers. Construction and Building Materials; 17(5), 339-351.

Circolare, C.S.L.L.P.P. 617 2009. Istruzioni per l'applicazione delle Norme Tecniche per le Costruzioni di cui al DM 14 gennaio 2008. Gazzetta Ufficiale della Repubblica Italiana 2009.

Collins, M. P. and Kuchma, D. [1999] "How Safe Are Our Large, Lightly Reinforced Concrete Beams, Slabs, and Footings?", ACI Structural Journal 96(4).

De Risi, R., Di Sarno, L., Paolacci, F. [2017] "Probabilistic seismic performance assessment of an existing RC bridge with portal-frame piers designed for gravity loads only", Engineering Structures 145, 348-367.

Delgado, R., Delgado, P., Pouca, N. V., Arêde, V., Rocha, P., Costa, A. [2009] "Shear effects on hollow section piers under seismic actions: experimental and numerical analysis", Bulletin of Earthquake Engineering 7(2), 377-389.

Elwood, K. J. [2004] "Modelling failures in existing reinforced concrete columns", Canadian Journal of Civil Engineering 31(5), 846-859.

Elwood, K. J., and Moehle, J. P. (2004). Evaluation of existing reinforced concrete columns. In Proceedings, 13th World Conference on Earthquake Engineering, Vancouver.

Fardis, M. N. and Pinto, P. E. "LESSLOSS–Risk mitigation for earthquakes and landslides. Guidelines for displacement-based design of buildings and bridges", Report n 5/2007.

Federation Internationale du Beton. Seismic bridge design and retrofit – structural solutions. FIB Bulletin 39, 2007.

FHWA-HRT-06-032: Buckle, I., Friedland, I., Mander, J., Martin, G., Nutt, R., Power, M. [2006] "Seismic retrofitting manual for highway structures: Part 1 – bridges", Federal Highway Administration, McLean, Virginia.

Hiraishi H. Evaluation of shear and flexural deformations of flexural type shear walls. Bull New Zealand Soc Earthq Eng 1984;17(2):135-144.

Hoshikuma, J. I. and Priestley, M. J. N. [2000] "Flexural behavior of circular hollow columns with a single layer of reinforcement under seismic loading", SSRP; 13. University of California, San Diego.

Jensen, U. G. and Hoang L. C. [2010] "Shear Strength of Reinforced Concrete Piers and Piles with Hollow Circular Cross Section", Structural Engineering International 20(3), 260-267.

Jensen, U. G. and Hoang, L. C. [2009] "Shear strength prediction of circular members by the Crack Sliding Model", Magazine of Concrete Research 61(9), 691–703.

Kim, I. H., Sun, C. H., Shin, M. [2012] "Concrete contribution to initial shear strength of RC hollow bridge columns", Structural Engineering and Mechanics 41(1): 43-65.

Kishida, S., Horii, M., Kuwabara, F., Hayashi, S. [1998] "Experimental study on shear strength of the PHC pile with large diameter", Journal of Structural and Construction Engineering 8(519), 123–130 (in Japanese).

Kowalsky, M.J. and Priestley, M.N. [2000] "Improved analytical model for shear strength of circular reinforced concrete columns in seismic regions", ACI Structural Journal 97(3).

Lee, J. H., Choi, J. H., Hwang, D. K., Kwahk, I. J. [2015] "Seismic performance of circular hollow RC bridge columns", KSCE Journal of Civil Engineering, 19(5), 1456-1467.

Mander, J. B., Priestley, M. J. N., and Park, R. [1988]. "Theoretical stress-strain model for confined concrete." Journal of Structural Engineering ASCE, 114(8), 1804-1825.

McKenna F., Fenves G.L., Scott M.H. [2000] "Open system for earthquake engineering simulation", available at http://opensees.berkeley.edu.

Ohtaki, T. [2000] "An experimental study on scale effects in shear failure of reinforced concrete columns", Strain 500(500), 36-D13.

Pinto, P. E., Franchin, P., Lupoi, A., Mancini, G., Pavese, A., Spacone, E., Vulcano, A. [2005] "Linee guida e manuale applicativo per la valutazione della sicurezza sismica e il consolidamento dei ponti esistenti in ca.", Progetto DPC-Reluiss, 2008. (in italian)

Priestley, M. J.N., Calvi, G. M., Kowalsky, M. J. [2007] Displacement-based seismic design of structures, IUSS press, Pavia, Italy.

Priestley, M. J. N., Seible, F., Calvi, G. M. [1996] Seismic design and retrofit of bridges, John Wiley & Sons, New York.

Priestley, M. J. N., Verma, R., Xiao, Y. [1994] "Seismic shear strength of reinforced concrete columns", ASCE Journal of Structural Engineering, 120(8), 2310-2329.

Priestley, M. J. N. [2003] Myths and fallacies in earthquake engineering. Revisited. IUSS press, Pavia, Italy.

Ranzo, G., Priestley, M. J. N. [2001] "Seismic performance of circular hollow columns subjected to high shear", SSRP 2001, 1. University of California, San Diego.

Regis, P. [1990] "Resistência ao Esforço Cortante em Peças de Concreto Armado com Seção Circular Vazada", Tese de M.Sc, COPPE/UFRJ, Rio de Janeiro-RJ.

Sezen, H., Mohele, J. P. [2004] "Shear Strength Model for Lightly Reinforced Concrete Columns", ASCE Journal of Structural Engineering 130(11), 1692-1703.

STRIT RT D.1.2 – part 1. Inventory e sviluppo database per la caratterizzazione della vulnerabilità delle infrastrutture viarie. STRIT Project PON Ricerca e Competitività 2007-2013, 2015.

Turmo, J., Ramos, G., Aparicio, A. C. [2009] "Shear truss analogy for concrete members of solid and hollow circular cross section", Engineering Structures 31(2), 455-465.

Völgyi, I., Windisch, A., Farkas, G. [2014] "Resistance of reinforced concrete members with hollow circular cross-sections under combined bending and shear–Part I: experimental investigation", Structural Concrete 15(1), 13-20.

Völgyi, I., Windisch, A. [2014] "Resistance of reinforced concrete members with hollow circular cross- section under combined bending and shear–Part II: New calculation model", Structural Concrete 15(1), 21-29.

Whittaker, D., Park, R., Carr, A. J. [1987] "Experimental tests on hollow circular concrete columns for use in offshore concrete platforms". Proc. Of the Third Pacific Conference on Earthquake Engineering, Vol. 1, New Zeland.

Yeh, Y. K., Mo, Y. L., Yang, C. Y. [2001] "Seismic performance of hollow circular bridge piers", ACI Structural Journal 98(6), 862-871.

Yoshimura, M., and Yamanaka, N. [2000] "Ultimate Limit State of RC Columns", Second US Japan Workshop on Performance-Based Earthquake Engineering Methodology for Reinforced Concrete Building Structures, Sapporo, Japan, PEER report 2000/10. Berkeley, Calif.: Pacific Earthquake Engineering Research Center, University of California, pp. 313-326.

Zahn, F. A., Park, R., Priestley, M. J. N., [1990] "Flexural Strength and Ductility of Circular Hollow Reinforced Concrete column without Confinement on Inside Face", ACI Structural Journal 87(2), 156-166.

Zhang, J. P. [1997] "Diagonal cracking and shear strength of reinforced concrete beams", Mag. Concr. Res. 49(178): 55–65.

Test ID	D_e (mm)	L_V (mm)	L_V/D_e (-)	t_w (mm)	ρ_l (%)	ρ_w (%)
PC1	550	1650	3.00	100	0.85	0.06
PC2		1100	2.00			

Table 1: Main geometrical properties of tested specimens

Concrete	Steel			
f_c (MPa)	d_b (mm)	f_y (MPa)	f_t (MPa)	f_t/f_y (-)
15.6	8	540	620	1.15
	3	655	690	1.05

Table 2: Mechanical properties of the adopted materials

Cycle	DR (%)	μ' (-)	Description of the observed damage
1	0.20		Horizontal hairline cracks on the west and east faces
2	0.43		Spread of horizontal cracks along specimen's height
3	0.67	1.4	First slight diagonal cracks
4	0.91	2.0	Increase in width of existing cracks and new diagonal cracks
5	1.91	4.1	Longitudinal bars buckling and concrete cover spalling near to base section on west face
6	2.92	6.3	Significant buckling of longitudinal bars and concrete spalling
7	3.91	8.4	Complete concrete cover spalling, severe buckling of longitudinal bars and wide diagonal cracks
8	4.93	10.6	Failure in tension of the outer longitudinal bars due to oligo-cyclic fatigue

Table 3: Summary of the damage evolution during Test PC1

Cycle	DR (%)	μ' (-)	Description of the observed damage
1	0.16		Horizontal hairline cracks on west and east sides
2	0.37		First slight diagonal cracks on north and south sides
3	0.60	1.2	Increasing in width of existing cracks and new diagonal cracks
4	0.83	1.6	Widening of existing main shear cracks
5	1.82	3.6	Concrete cover spalling in a small portion near to the base section along the east/west direction
6	2.87	5.7	Sudden widening of the main diagonal crack

Table 4: Summary of the damage evolution during Test PC2

Test ID	L_V/D_e (-)	$V'^{(+)}_y$ (kN)	$DR'^{(+)}_y$ (%)	$V'^{(-)}_y$ (kN)	$DR'^{(-)}_y$ (%)	$V^{(+)}_{max}$ (kN)	$DR^{(+)}_{max}$ (%)	$V^{(-)}_{max}$ (kN)	$DR^{(-)}_{max}$ (%)	$DR^{(+)}_u$ (%)	$DR^{(-)}_u$ (%)	FM_{exp}
PC1	3.0	+86.7	+0.49	-86.4	-0.44	+108.2	+1.91	-102.4	-1.87	4.18	-4.30	F
PC2	2.0	+138.0	+0.49	-133.6	-0.52	+166.9	+1.78	-147.1	-1.80	2.55	-	FS

Table 5: Yielding, peak and ultimate values of lateral load and drift; observed failure modes

	f_c (MPa)	f_y (MPa)	$\rho_l = A_l/A_c$ (-)	f_{yw} (MPa)	$\rho_w = n_\Phi A_\Phi/(2t_w\, s)$ (-)	$N/A_c f_c$ (-)	s/D_e (-)	L_V/D_e (-)
Max	16.0	418.0	0.85	392.0	0.00	0.00	0.05	2.00
Min	40.0	600.0	5.33	655.0	0.40	0.27	0.50	2.55

Table 6: Ranges of variability for the main properties of the collected experimental tests

Test	LT*	TT**	D_e (mm)	D_i (mm)	t_w (mm)	L_V (mm)	s [p]*** (mm)	ρ_l (%)	ρ_w (%)	f_c (MPa)	f_y (MPa)	f_{yw} (MPa)	$N/A_c f_c$ (-)	V_{test} (kN)	V'_y (kN)	FM_{ex} (-)
PA1	M	C	300	180	60	750	-	5.33	0.00	34.2	600	-	0.00	55	139	S
PA2	M	C	300	180	60	750	-	5.33	0.00	32.7	600	-	0.27	83	173	S
PB1	M	C	300	180	60	750	150	5.33	0.35	35.5	600	600	0.00	130	134	S
PB2	M	C	300	180	60	750	150	5.33	0.35	37.0	600	600	0.24	158	169	S
HS2	C	H	1524	1244	139	3880	70	2.25	0.33	40.0	450	635	0.05	1396	907	FS
HS3	C	H	1524	1244	139	3880	70	2.25	0.33	35.0	450	635	0.15	1457	1192	FS
PI2-C	C	C	1500	900	300	3500	200	2.15	0.26	30.9	418	410	0.10	2299	1618	FS
PI2-C*	C	C	1500	900	300	3500	200	2.15	0.26	33.2	423	392	0.10	2341	1699	FS
Test 1	M	C	600	400	100	1375	300	2.40	0.09	32.2	500	500	0.00	233	241	S
Test 2	M	C	600	400	100	1375	300	2.40	0.09	32.2	500	500	0.00	239	241	S
Test 3	M	C	600	400	100	1375	300	2.40	0.09	24.7	500	500	0.00	237	238	S
Test 4	M	C	600	400	100	1375	300	2.40	0.09	24.7	500	500	0.00	217	238	S
PC2	C	C	550	350	100	1100	120	0.85	0.06	15.6	540	655	0.05	150	129	FS

Loading Typology (LT): monotonic (M) or cyclic (C)
**Transverse reinforcement Typology (TT): circular (C) or helicoidal (H)
***Stirrups spacing (s) for C- transverse reinforcement typology; helicoidal pitch for H- reinforcement typology

Table 7: Main properties of the specimens belonging to the collected database

Shear strength model	DR_y	μ	θ
[Ranzo and Priestley, 2001] (RP)	$DR_y = DR'_y \frac{M_n}{M'_y}$	$\mu_{max} = \frac{DR_{test}}{DR_y} = \frac{DR_{test}}{DR'_y}\frac{M'_y}{M_n}$	30°
[Ranzo and Priestley, 2001] with V_w by [Turmo et al., 2009] (RP+T)	$DR_y = DR'_y \frac{M_n}{M'_y}$	$\mu_{max} = \frac{DR_{test}}{DR_y} = \frac{DR_{test}}{DR'_y}\frac{M'_y}{M_n}$	30°
[Jensen and Hoang, 2010] (JH)	-	-	$\text{arctg}\left(\frac{D_e}{m}\right)$
[EC8-3, 2005] (EC8)	$DR_y = \theta_{y,P\&F}$	$\mu_s = \frac{DR_s}{DR_y} = \frac{DR_s}{\theta_{y,P\&F}}$	45°
[C617, 2009] (C617)	$DR_y = DR'_y \frac{M_n}{M'_y}$	$\mu_{max} = \frac{DR_{test}}{DR_y} = \frac{DR_{test}}{DR'_y}\frac{M'_y}{M_n}$	30°
[FHWA, 2006] (FHWA)	-	-	From Eq. (12)

Table 8: Details for application of the analysed shear strength models

					RP		*RP+T*		*JH*		*EC8*		*C617*		*FHWA*	
Authors	Specimen	LT	V_{test} (kN)	FM_{exp} (-)	FM (-)	V_{pred}/V_{test} (-)	FM (-)	V_{pred}/V_{test} (-)	FM (-)	V_{pred}/V_{test} (-)	FM (-)	V_{pred}/V_{test} (-)	FM (-)	V_R/V_{test} (-)	FM (-)	V_{pred}/V_{test} (-)

[Regis, 1990]	PA1	M	55	S	S	0.77	S	0.77	S	0.87	S	2.46	S	1.12	S	1.15
	PA2	M	83	S	S	1.03	S	1.03	S	0.55	S	2.17	S	1.31	S	1.34
	PB1	M	130	S	S	0.81	S	0.94	S	0.85	S	1.41	S	0.92	S	1.22
	PB2	M	158	S	S	0.89	S	0.98	S	0.72	S	1.49	S	1.08	S	1.34
[Ranzo and Priestley, 2001]	HS2	C	1396	FS	FS	1.11	F	1.30	-	-	FS	1.05	FS	0.84	-	-
	HS3	C	1457	FS	FS	1.27	F	1.44	-	-	F	1.22	F	1.37	-	-
[Yeh et al., 2001]	PI2-C	C	2299	FS	FS	0.95	FS	1.06	-	-	FS	0.96	FS	0.76	-	-
[Cheng et al., 2003]	PI2-C*	C	2341	FS	FS	0.94	FS	1.05	-	-	FS	0.95	FS	0.80	-	-
[Turmo et al., 2009]	Test 1	M	233	S	S	0.85	S	0.92	S	0.93	S	1.10	S	1.10	S	1.30
	Test 2	M	239	S	S	0.83	S	0.89	S	0.91	S	1.07	S	1.08	S	1.26
	Test 3	M	237	S	S	0.76	S	0.82	S	0.79	S	0.97	S	0.98	S	1.17
	Test 4	M	217	S	S	0.83	S	0.90	S	0.86	S	1.06	S	1.07	S	1.27
Authors' test	PC2	C	150	FS	S	0.74	FS	0.83	-	-	S	0.65	FS	0.79	-	-
All					Mean	**0.91**	Mean	**1.00**	Mean	**0.81**	Mean	**1.27**	Mean	**1.02**	Mean	**1.26**
					COV	**0.17**	COV	**0.19**	COV	**0.15**	COV	**0.40**	COV	**0.19**	COV	**0.06**
S					Mean	**0.85**	Mean	**0.91**	Mean	**0.81**	Mean	**1.47**	Mean	**1.08**	Mean	**1.26**
					COV	**0.10**	COV	**0.09**	COV	**0.15**	COV	**0.38**	COV	**0.10**	COV	**0.06**
FS					Mean	**1.00**	Mean	**1.14**	Mean	-	Mean	**0.96**	Mean	**0.91**	Mean	-
					COV	**0.20**	COV	**0.21**	COV	-	COV	**0.21**	COV	**0.28**	COV	-

Table 9: Comparison between predicted (V_{pred}) and experimental (V_{test}) shear strength and failure mod

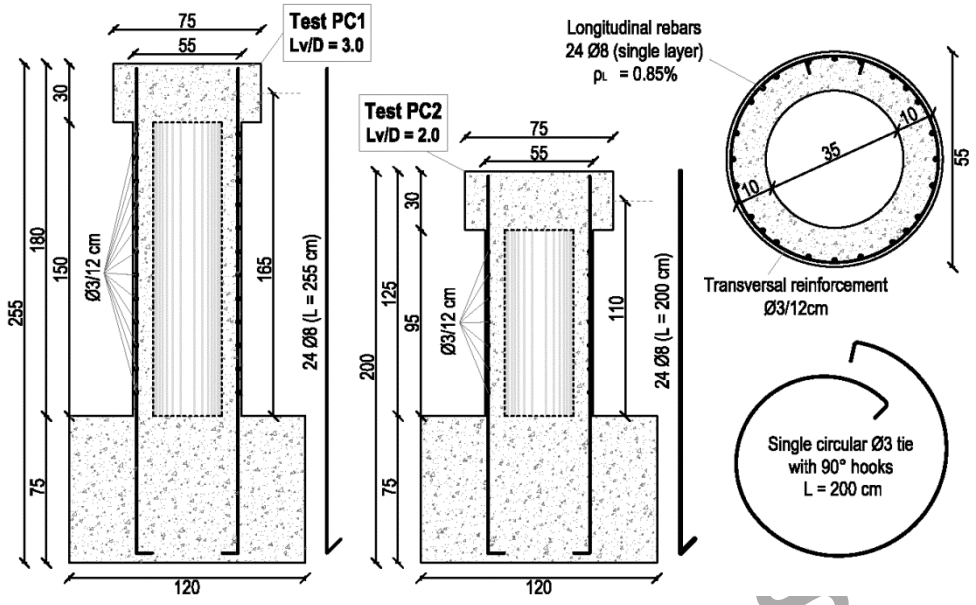

Figure 1: Geometry and reinforcement details (quota in centimetres)

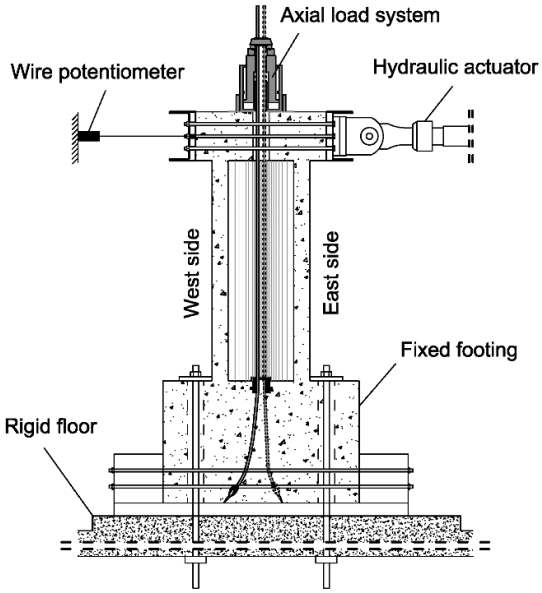

(a)

(b)

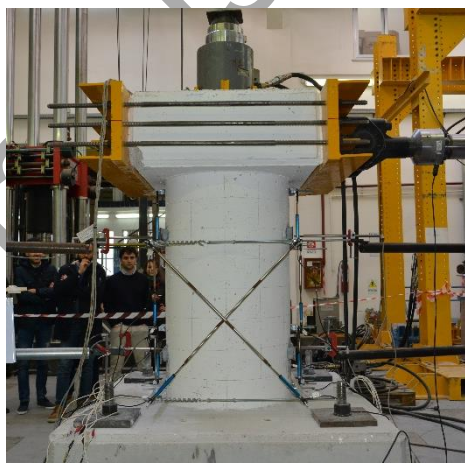

(c)

Figure 2: Schematic view of the test setup (a); photos of tests PC1 (b) and PC2 (c)

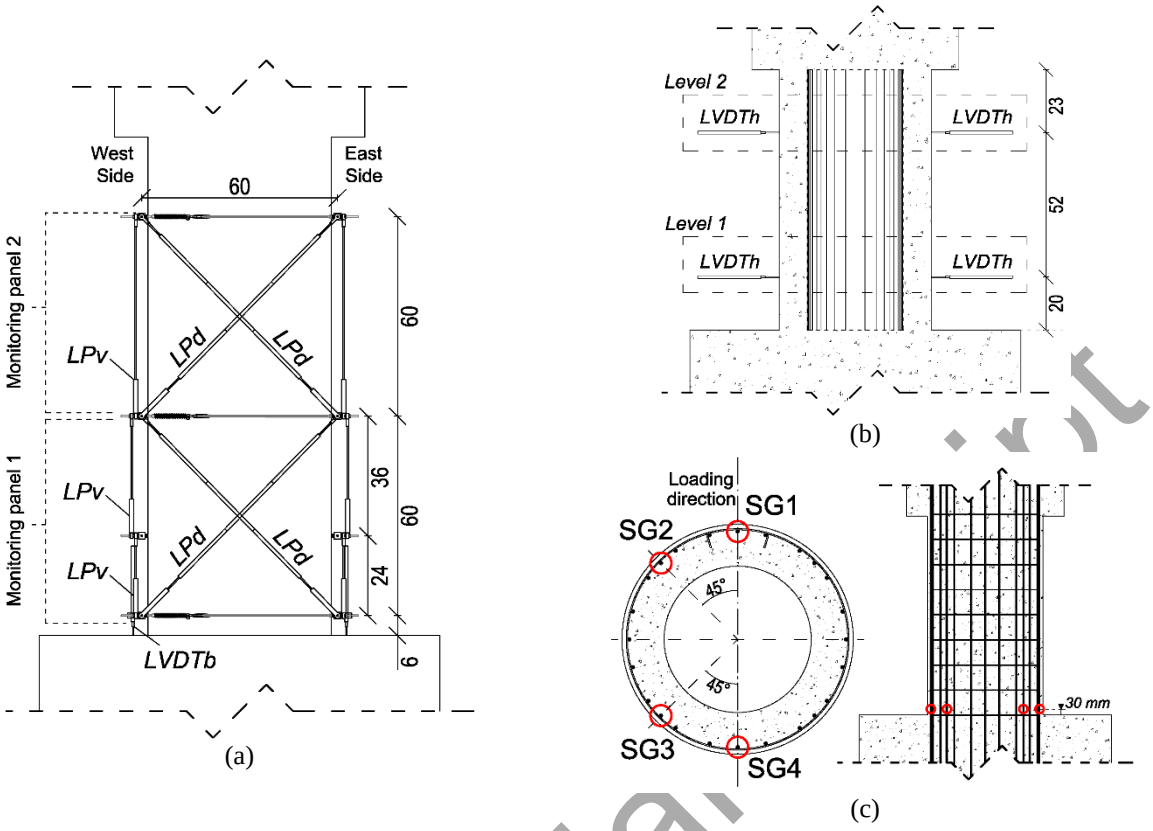

Figure 3: Monitoring system: LPs and LVDTs (a), Horizontal LVDT for test PC2 (b), and SGs (c)

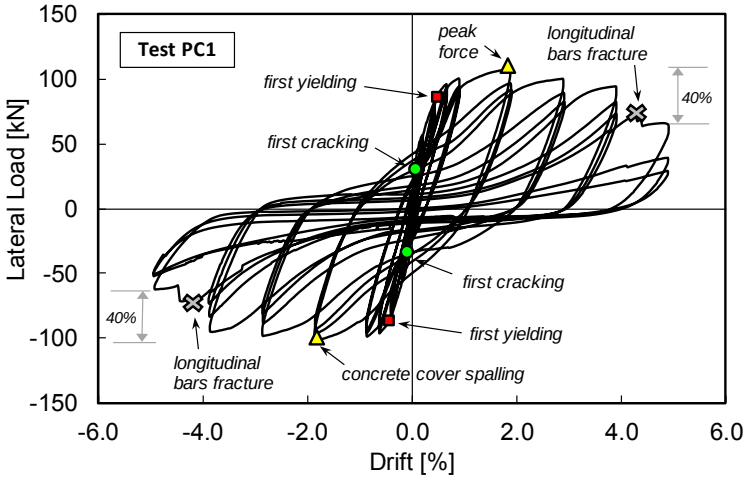

Figure 4: Lateral load versus drift response - Test PC1

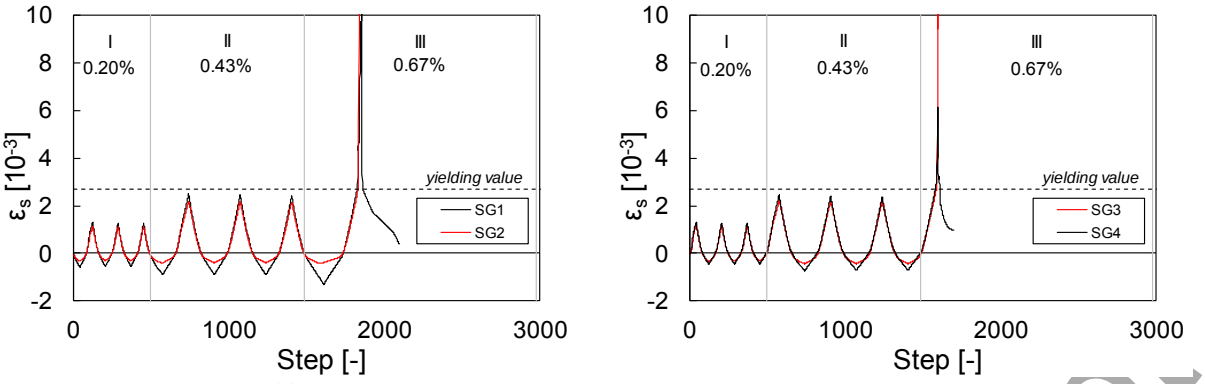

Figure 5: Strains of longitudinal west (a) and east (b) bars for Test PC1

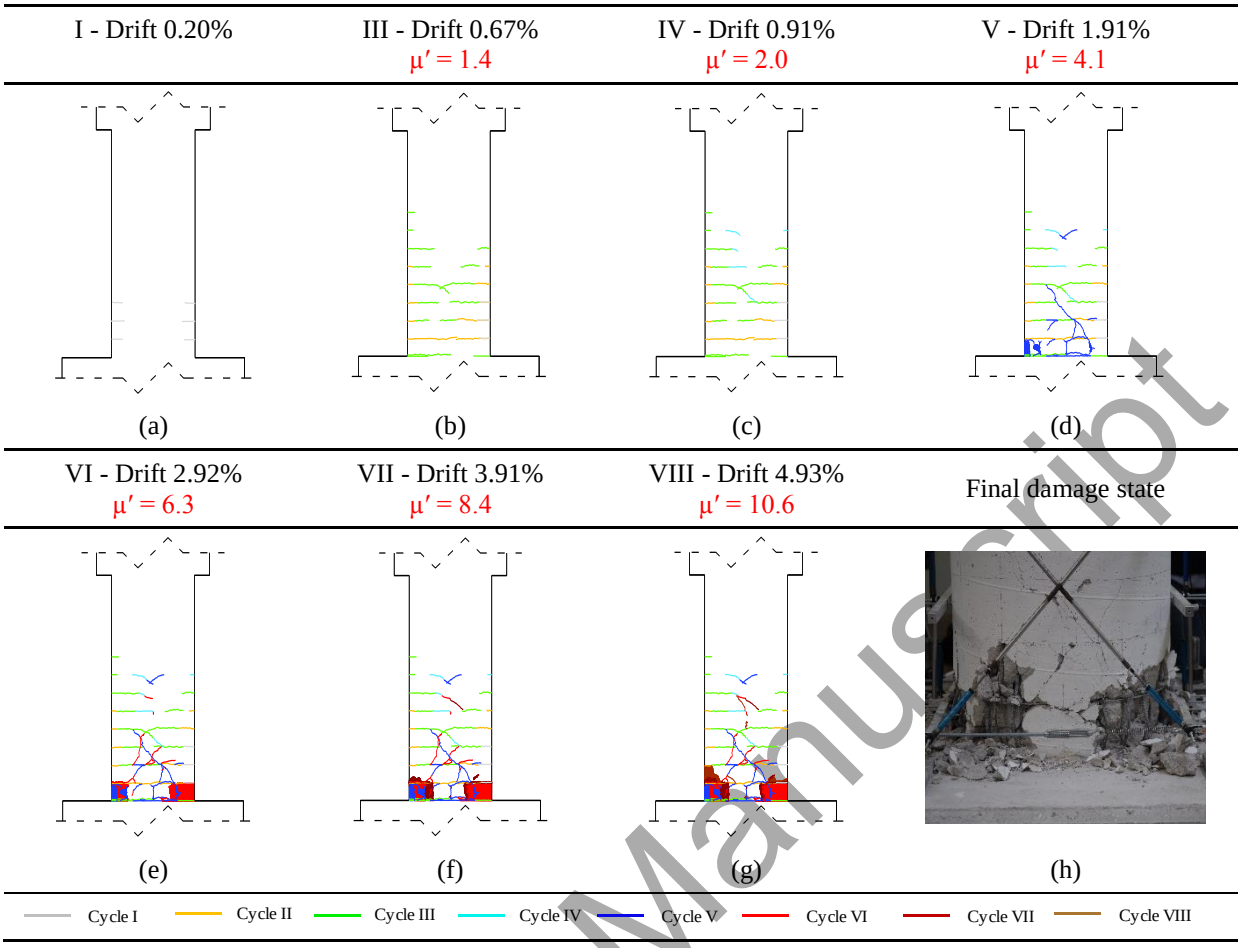

Figure 6: Damage evolution for Test PC1

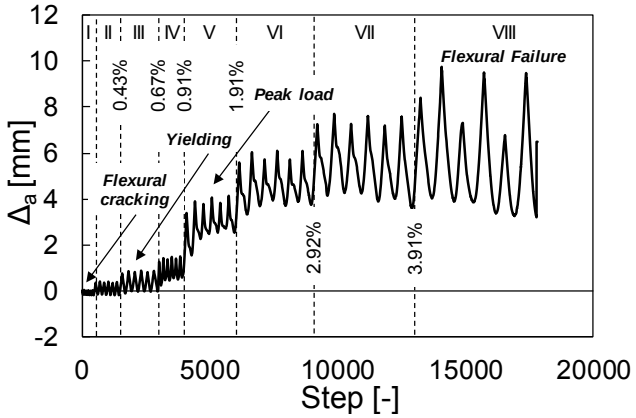

Figure 7: Hydraulic jack elongation (i.e. column shortening) for Test PC1

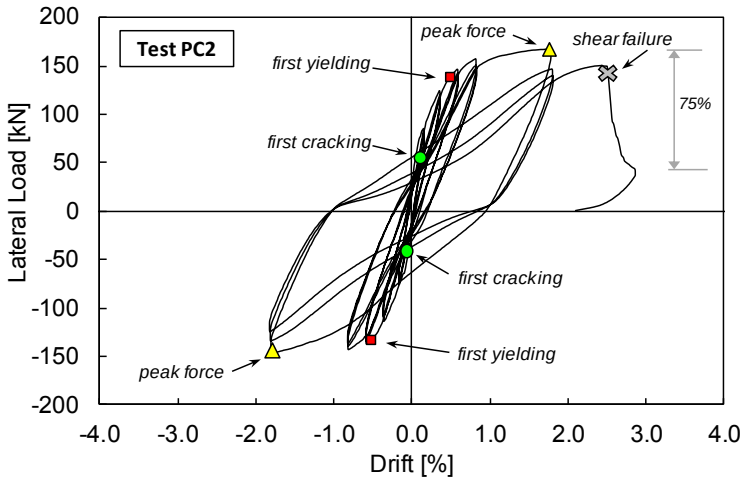

Figure 8: Lateral load versus drift response - Test PC2

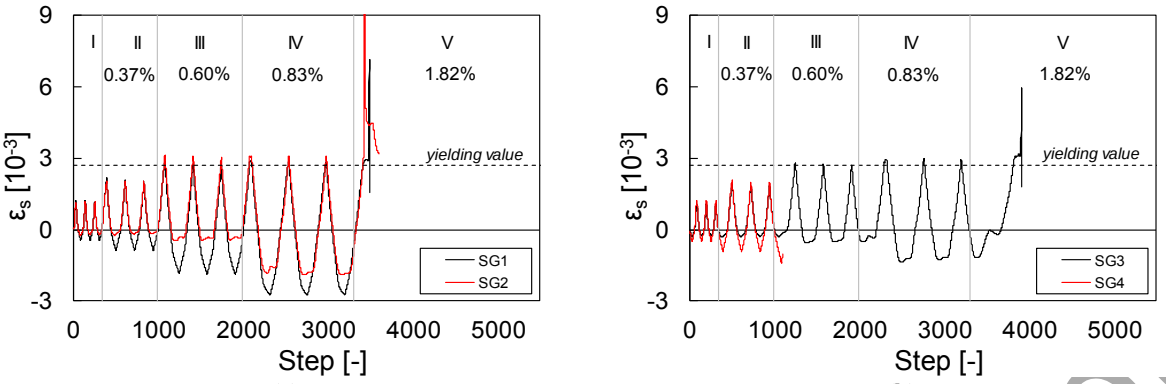

(a) (b)

Figure 9: Strains of longitudinal west (a) and east (b) bars for Test PC2

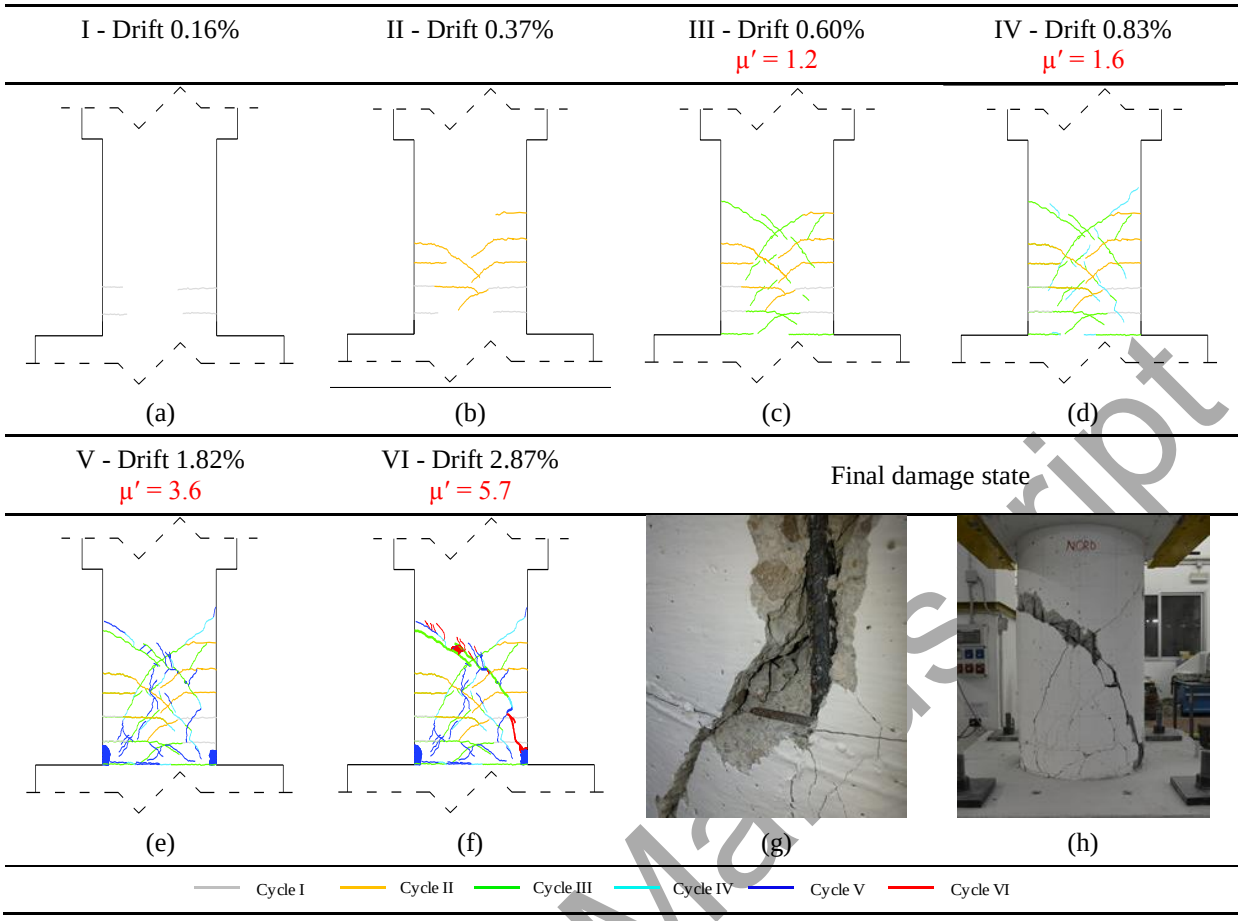

Figure 10: Damage evolution for Test PC2 (a-f), circular tie failure in tension and dowel bar deformation (g), final damage state (h)

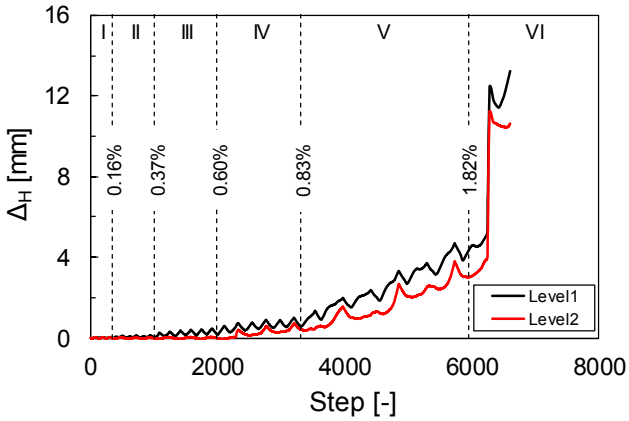

Figure 11: Evolution of the horizontal component Δ_H of shear cracks width during test PC2

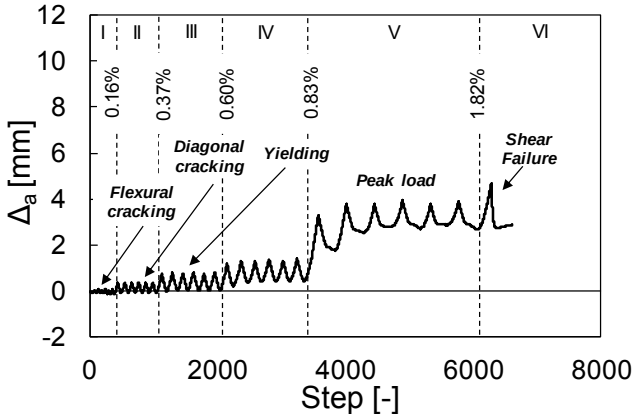

Figure 12: Hydraulic jack elongation (i.e. column shortening) for Test PC2

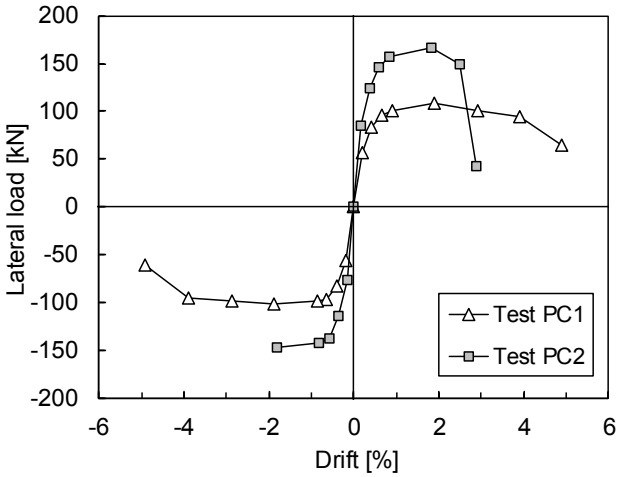

Figure 13: Comparison of first-cycle envelopes

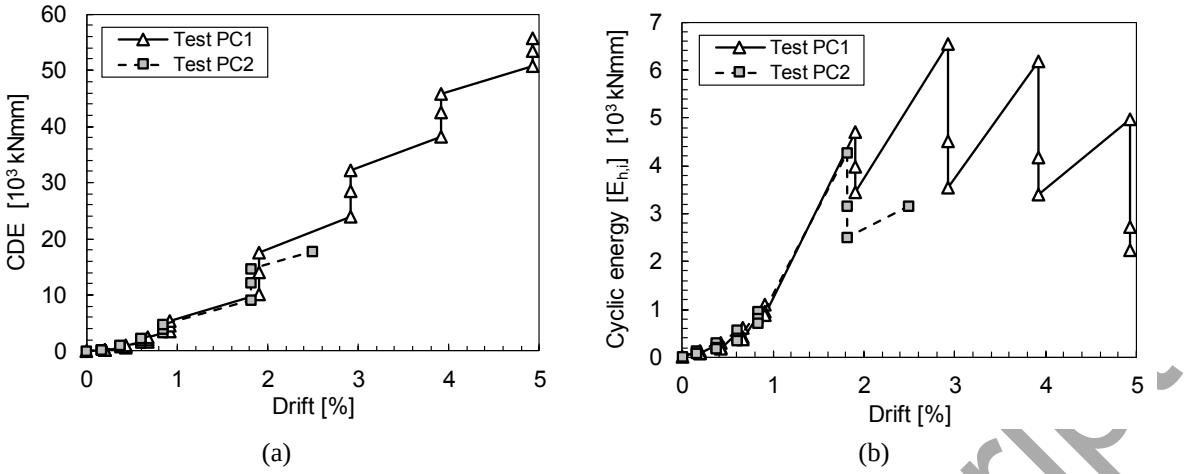

(a) (b)

Figure 14: Cumulative dissipated energy (a), and energy dissipation at each cycle (b)

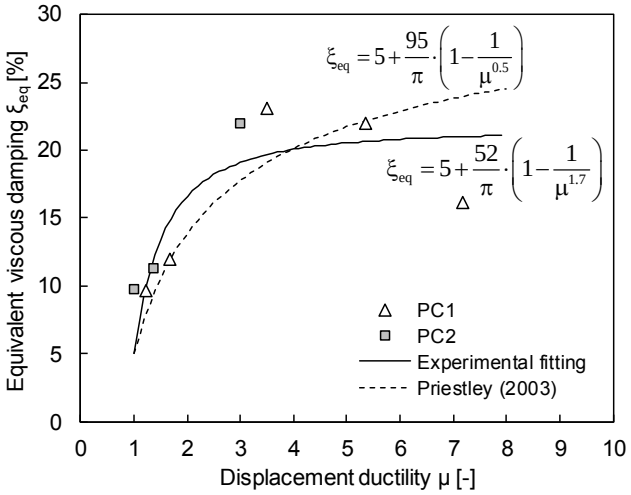

Figure 15: Equivalent viscous damping for tests PC1 and PC2 depending on displacement ductility demand

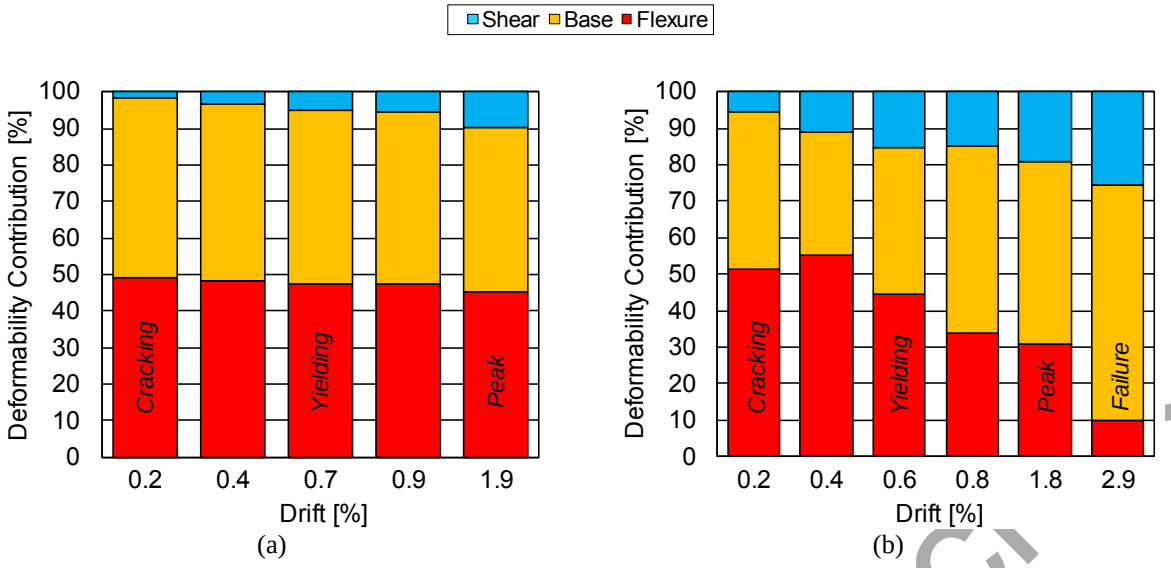

Figure 16: Deformability contributions to the overall top displacement: Test PC1 (a) and Test PC2 (b)

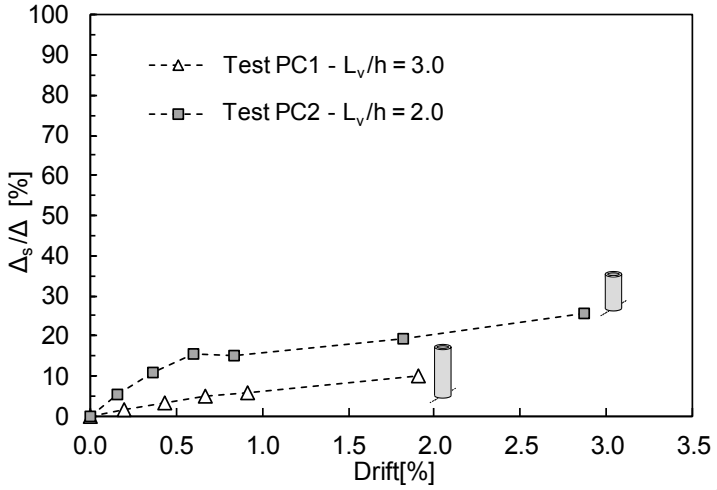

Figure 17: Shear deformability contribution to the overall top displacement

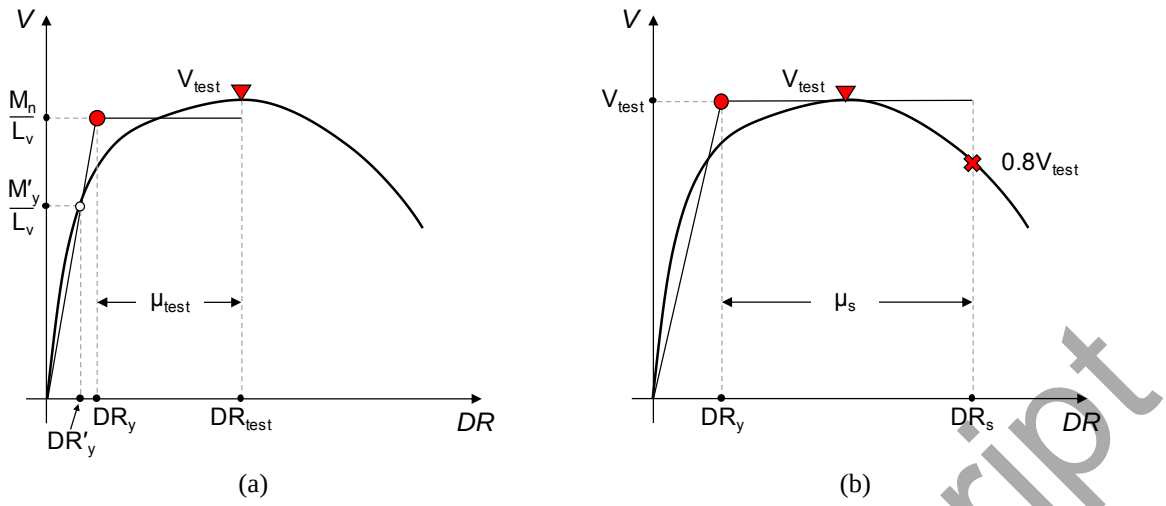

Figure 18: Characteristic points on the experimental envelope – calculation of yielding drift DR_y according to [Ranzo and Priestely, 2001] (a) and [Biskinis et al., 2004] (b)

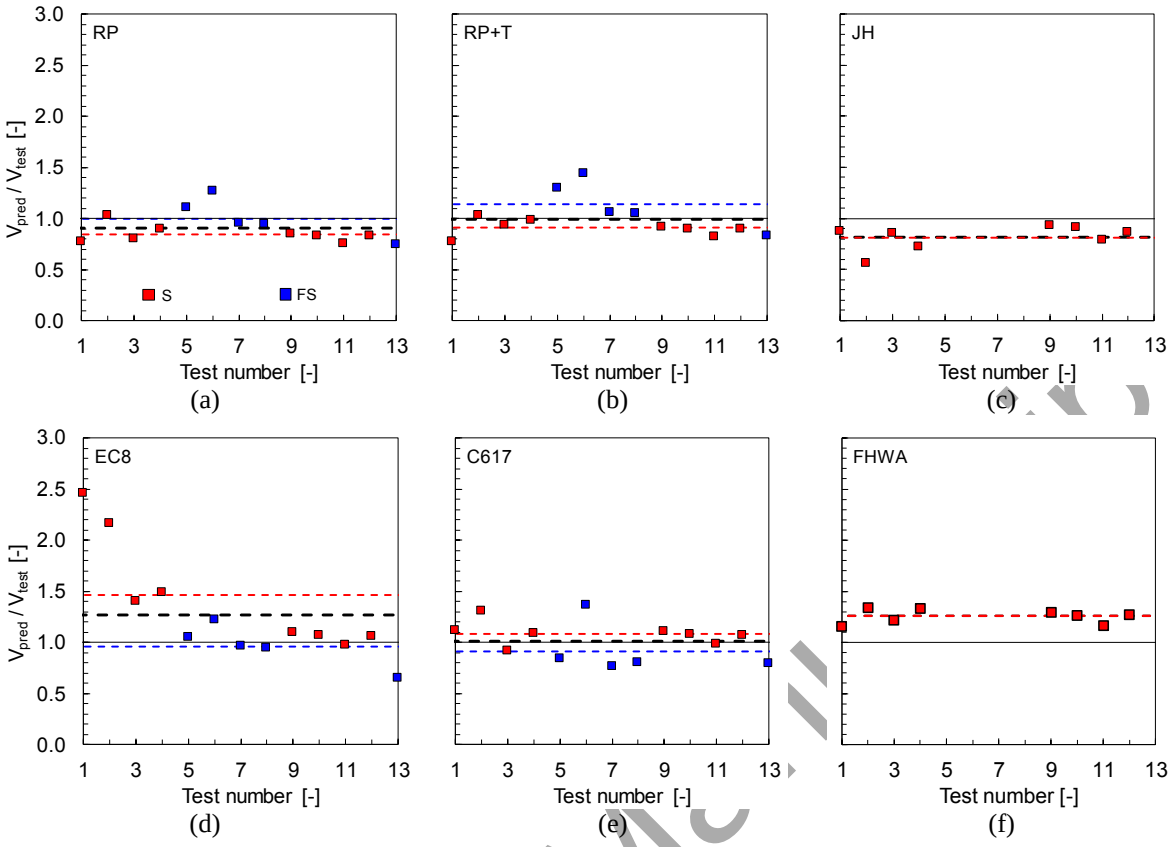

Figure 19: Comparison between predicted and experimental shear strength values